Title

A Genetically Defined Circuit for Arousal from Sleep during Hypercapnia.

Journal

Neuron, 96(5)

ISSN

0896-6273

Authors

Kaur, Satvinder
Wang, Joshua L
Ferrari, Loris
et al.

Publication Date

2017-12-01

DOI

10.1016/j.neuron.2017.10.009

Peer reviewed

HHS Public Access

Author manuscript

Neuron. Author manuscript; available in PMC 2018 December 06.

Published in final edited form as:

Neuron. 2017 December 06; 96(5): 1153–1167.e5. doi:10.1016/j.neuron.2017.10.009.

A Genetically-Defined Circuit for Arousal from Sleep during Hypercapnia

Satvinder Kaur[1], **Joshua L Wang**[1], **Loris Ferrari**[1], **Stephen Thankachan**[2], **Daniel Kroeger**[1], **Anne Venner**[1], **Michael Lazarus**[3], **Andrew Wellman**[4], **Elda Arrigoni**[1], **Patrick M Fuller**[1], and **Clifford B Saper**[1,*]

[1]Department of Neurology, Program in Neuroscience, Beth Israel Deaconess Medical Center and Harvard Medical School, Boston, Massachusetts, 02215, USA

[2]Department of Psychiatry, Harvard Medical School & VA Boston healthcare, 1400 VFW Parkway, West Roxbury, MA 02132

[3]International Institute for Integrative Sleep Medicine (WPI-IIIS), University of Tsukuba, 1-1-1 Tennodai, Tsukuba, 305-8575, Japan

[4]Division of Sleep and Circadian Disorders, Departments of Medicine and Neurology, Brigham and Women's Hospital, Harvard Medical School, Boston, MA

Summary

The precise neural circuitry that mediates arousal during sleep apnea is not known. We previously found that glutamatergic neurons in the external lateral parabrachial nucleus (PBel) play a critical role in arousal to elevated CO2 or hypoxia. Because many of the PBel neurons that respond to CO2 express calcitonin gene-related peptide (CGRP), we hypothesized that CGRP may provide a molecular identifier of the CO2 arousal circuit. Here we report that selective chemogenetic and optogenetic activation of $PBel^{CGRP}$ neurons caused wakefulness, whereas optogenetic inhibition of $PBel^{CGRP}$ neurons prevented arousal to CO2, but not to an acoustic tone or shaking. Optogenetic inhibition of $PBel^{CGRP}$ terminals identified a network of forebrain sites under the control of a $PBel^{CGRP}$ switch that is necessary to arouse animals from hypercapnia. Our findings define a novel cellular target for interventions that may prevent sleep fragmentation and the attendant cardiovascular and cognitive consequences seen in obstructive sleep apnea.

Patients with obstructive sleep apnea suffer from repeated cycles of upper airway collapse during sleep, causing apnea (with increases in CO2, hypercapnia, and fall in O2, hypoxia), followed by arousal that re-establishes the airway. Although the arousals are brief and

*Lead Contact, corresponding author: Contact, Clifford B. Saper, M.D., Ph. D., Beth Israel Deaconess Medical, Center, Department of Neurology, 330 Brookline Ave, Boston, MA 02215, Phone: 617-667-2622, csaper@bidmc.harvard.edu.

Contribution of authors: SK: experimental design, data collection and analysis, manuscript writing; JW- data scoring and analysis; LF and EA- in vitro data collection, analysis and manuscript writing; ST and DK- data collection and analysis in optogenetics and imaging; AV- data analysis and presentation, AW- Respiratory analysis; ML and PF- generation and validation of the AAV's used in the study, CBS- experimental design and manuscript writing

lifesaving in the short term, the sleep fragmentation they cause prevents the patient from entering deeper states of sleep (Bonsignore et al., 2012;Mannarino et al., 2012), causing subsequent daytime sleepiness and increasing risk of cardiovascular and metabolic disease in the long term (Ayalon and Peterson, 2007;Benarroch, 2007). Dissociating the arousal from sleep from the increase in respiratory drive that reinitiates breathing could potentially prevent this outcome (Berry and Gleeson, 1997), but will require understanding the circuits that mediate both aspects of the response to apnea.

In our previous work, we showed that glutamatergic neurons in the lateral parabrachial region are required for the arousal response to hypercapnia, hypoxia, or the combination of the two. In particular, it appeared that neurons in the external lateral parabrachial subnucleus (PBel) were necessary for this response (Kaur et al., 2013). The PBel is an attractive candidate for causing arousal during apnea, as it projects extensively to the lateral hypothalamus, basal forebrain, and amygdala (Bernard et al., 1993;Saper, 1982;Saper and Loewy, 1980). However, there are many other glutamatergic neurons in the parabrachial region that project to the forebrain, as well as ones in the neighboring lateral crescent and Kolliker-Fuse nuclei that project extensively to the medulla and spinal cord (Herbert et al., 1990;Yokota et al., 2015), and may be responsible for augmenting respiration during hypoxia or hypercapnia. Finding a genetic differentiation between the neurons responsible for forebrain arousal during apnea and those that augment respiration would allow us to manipulate these cell groups selectively.

We and others had previously found that many of the neurons of the PBel, express calcitonin gene-related peptide (CGRP) (Yasui et al., 1989). CGRP neurons are found in the PBel as well as its forebrain targets in a variety of mammals including mice (Campos et al., 2016) and humans (deLacalle S. and Saper, 2000). The $PBel^{CGRP}$ neurons are known to receive both pain and visceral sensory information (Carter et al., 2013;Carter et al., 2015;deLacalle S. and Saper, 2000), and to show cFos activation in response to hypercapnia (Yokota et al., 2015). Therefore, we hypothesized that the $PBel^{CGRP}$ neurons may be important for relaying aversive signals, such as those that accompany hypercapnia, to the forebrain to cause arousal. To test this hypothesis, we used inducible CGRP-CreER mice (Song et al., 2012), where CreER encodes a fusion protein of Cre recombinase and estrogen receptor (ER), and CreER is transported to the nucleus of the cell only when an estrogen receptor ligand such as tamoxifen (TM) is present. Thus, TM administration to CGRP-CreER mice provides an efficient means for temporal gating of Cre expression.

In the present study we combined temporal control of Cre expression with intracranial injections of adeno-associated viral vectors (AAVs) containing Cre-dependent expression cassettes for either the activating hM3Dq receptor or the inhibitory opsin archaerhodopsin TP009 (Arch T). This allowed us to test, for the first time, the effects of selectively manipulating the $PBel^{CGRP}$ neurons on the arousal response to hypercapnia as well as define the downstream forebrain circuit network mediating the arousal response.

Results

Experiment 1 (activation of PBel^{CGRP} neurons)

We first wanted to test whether chemogenetic or optogenetic activation of PBel^{CGRP} neurons would be sufficient to cause arousal from a sleeping state. To allow selective activation of PBel^{CGRP} neurons, we first placed bilateral injections of AAV-FLEX-hM3Dq-mCherry into the PBel of six CGRP-CreER mice. In 5 out of 6 mice there was bilateral immunostaining in the PBel^{CGRP} neurons for the hM3Dq-mCherrry fusion protein (Fig. 1D–G). We compared the sleep in these mice after injection of saline (0.9%) or after two different concentrations of CNO (0.1 and 0.3 mg/kg). As expected, in the animals given saline, there was some wakefulness (55.8 ± 9.3%) in the first hour after saline injection, but once sleep was initiated it was maintained (an average of 57.9 ± 7.9 % NREM; 5.2 ± 1.3% REM sleep; and 36.9 ± 9.4% wakefulness in the first three hours) (Fig. 1I–K). A similar sleep pattern was also observed after administering 0.1mg/kg of CNO which was not significantly different from the saline group (Fig. 1H). However after the injection of CNO at 0.3 mg/kg, a significant increase of 54.4 ±11.3% in wakefulness compared to saline was seen in the first two hours. Wakefulness reached 98.1±1.6 % in the first hour, and 75.7 ± 11.8% in the second hour after 0.3mg/kg CNO, and was significantly higher than that after saline ($F_{2, 20}$= 26.4; P=0.02 overall comparison day/night X treatment groups (saline, two doses of CNO) Fig. 1H; $F_{23, 168}$= 4.06; P=0.04 for comparison across 24h; with P= 0.002 and P< 0.001 for the each of first two hours respectively) (Fig. 1I). Concomitant decreases in NREM sleep (96% and 68%; compared to saline) were significant during the first two hours after CNO, when only 1.7 ± 1.6% and 24.3 ± 11.9% of time was spent in NREM sleep ($F_{2, 20}$= 22.9; P=0.04 overall; $F_{23, 168}$= 4.26; P=0.04 for comparison of treatment groups across 24h; with P= 0.001 and P< 0.001 for the first two hours respectively, Fig. 1J). REM sleep was completely suppressed during the first three hours after injection of CNO at 0.3 mg/kg ($F_{2, 20}$= 7.2; P=0.014 overall; $F_{23, 168}$= 7.78; P=0.006 for comparison across 24h; with P= 0.003 and P= 0.01 for the second and third hours respectively, Fig. 1K). REM sleep rebounded in the fourth hour and thereafter animals showed a percentage of REM sleep in the range of 4–6% in the following three hours which was comparable to that after saline injections (Fig. 1K).

We also tested if acute stimulation of PBel^{CGRP} neurons can trigger arousal by optogenetic activation of these cells for 5 s during sleep. We found that blue laser (473 nm) light-induced activation of PBel^{CGRP} neurons with 10 ms pulses at 10 and 20 Hz (Fig. S1) can cause cortical arousal with significantly shorter latencies ($F_{7, 26}$= 26.06; P<0.001; Fig. S1E–F) than when compared to either the Laser-OFF group or the control group with only GFP expression. At 20 Hz, in animals with ChR2 expression in PBel and correct placement of the glass fiber (n=6), mice woke up in nearly all trials within the period of laser stimulation (5 sec) (Fig. S1F and G), as opposed to control mice expressing only GFP, where it was ineffective in waking up during the stimulus.

Experiment 2 (Photoinhibition of PBel^{CGRP} neurons)

In vitro demonstration that ArchT silences PBel^{CGRP} neurons—We next wanted to use ArchT to suppress the firing of PBel^{CGRP} neurons. We first tested ArchT using whole cell patch clamp recordings in the slice preparation. In current clamp mode, we found that

with ≈ +100 pA of current injection, we could bring the membrane potential of PBel neurons up above the threshold for firing. We then exposed the PBel^{CGRP} neurons expressing ArchT-GFP to 60 s pulses of 593 nm orange light. This produced a −13.82 ± 2.36 mV membrane hyperpolarization ($n = 5$; $p = 0.004$ paired t-test) and silenced the firing of the cells for the duration of the laser light exposure. The 593 nm light had no effect on the firing of PBel^{CGRP} neurons expressing GFP instead of Arch T (animals injected with AAV-Flex-GFP; $n = 5$) (Fig. 2H–J).

In vivo targeting of PBel^{CGRP} with ArchT—To test the effect of photoinhibiting PBel^{CGRP} neurons in vivo, we ablated the PBel CGRP neurons on one side of the brain, and transduced them with ArchT on the other side. This simplifies the placement of the optical fiber, as it only need be targeted accurately on one side of the brain. We therefore injected CGRP-CreER mice (Fig. 2A) unilaterally with an AAV-FLEX-mCherry-DTA vector that expresses diphtheria toxin A in neurons that contain Cre recombinase and mCherry in neurons that do not express Cre (so that the injection site can be identified). The DTA vector (Fig. 2B) caused nearly complete loss of CGRP neurons on that side of the brain (Fig. 2D and F), but no change in other local cell groups, which expressed mCherry (Fig. S2). We then injected the opposite side with AAV-FLEX-ArchT-GFP, which expresses ArchT in a Cre-dependent manner (Fig. S3). That same side was also targeted by a glass optical fiber to direct the laser light (Fig. 2E and G). The glass fibers were placed so that they sat directly on the surface of the pons over the PBel, but generally without penetrating the surface of the pons, so that no damage was done to the PBel. Out of 12 CGRP-CreER mice, 8 mice had the glass fiber accurately targeting the ArchT expressing cells in PBel.

Cortical arousals to hypercapnia—Arousal responses to hypercapnia were observed in all 8 of the CGRP-CreER mice with correct targeting of AAV-ArchT and the glass fiber. In the Laser-OFF condition the mean arousal latency was 16.5 ± 0.7sec (Fig. 2K and M). These animals awoke during the CO2 stimulus on every trial (0% failure to arouse), and similar latencies were also observed in the control (AAV-GFP) mice (15.3 ± 0.6 sec; n=4) with no ArchT expression and C57 wildtype mice with AAV-ArchT injections (16.4 ± 1.8 sec; n=6) (Fig. 2K and M). However, in the CGRP-CreER mice with correct targeting, in the Laser-ON condition, the arousal latency was increased fourfold (69.7 ± 6.7 sec; $F_{5, 29}$= 38.81; P< 0.001) (Fig. 2L and M) and in 49.8± 4.9% of the trials the mouse did not wake up during the 30 sec CO2 stimulus ($F_{5, 29}$= 52.1; P< 0.001) (Fig. 2N and O). In control mice with AAV-FLEX-GFP injections in the PBel (n=4) and no ArchT and in the C57 control mice (n=6) injected with AAV- ArchT (where no expression of ArchT was observed), the arousal latency did not differ with and without laser exposure and they also woke up with every trial of hypercapnia. In all trials that were measured, animals had been in NREM sleep for a minimum of 30 sec before onset of the trial, with a statistically comparable mean time in NREM before hypercapnia in Laser-ON (54.6 ± 3.3 sec) and Laser-OFF (50.8 ± 4.8 sec) conditions. These numbers were also similar to the normocapnic trials (below), in which the mean NREM duration prior to trial onset was 57.3 ± 2.8 sec, the mean time to arousal was 92.3 ± 5.6 sec, and the mean NREM sleep bout that extended across gas exchange trials was 149 sec.

Ventilatory response to hypercapnia—The respiratory signals acquired continuously with the EEG and EMG in the above experiment were analyzed offline. The flow signals were analyzed for respiratory rate, tidal volume, and ventilation using software to automatically detect the peaks and troughs of each breath for 90s of each of the CO2 trials. We then analyzed and compared the respiratory rate and tidal volume for the three breaths just before hypercapnia (Pre-CO2) to that of the three breaths just prior to when animals awoke in response to 10% CO2 in the Laser-OFF condition and then at the same time point in trials in the same animal with Laser-ON (in which the animals did not awaken). Our results show that the increase in breathing rate and tidal volume in response to CO2 was not significantly different in the Laser-ON or Laser-OFF conditions (Fig. S4). In other words, the inhibition of the PBel^{CGRP} neurons prevented the arousal, but not the ventilatory response to CO2.

Cortical arousals in normocapnia—In the presence of the normocapnic gas instead of CO2, the mean latency of arousal (representing the remaining duration of a normal NREM bout) was not significantly different between the Laser-ON (90.9 ± 8.3s) and Laser-OFF (94.8 ± 7.8s) (Fig. 3A–C) days. Similarly, the mean NREM bout lengths (including the NREM prior to the trial) for Laser ON (149.2 ± 8.8 sec) and Laser OFF (154.1 ± 7.7 sec) were also not significantly different. Also, laser inhibition of PBel^{CGRP} neurons did not affect the total amount of time spent in wake and sleep as the sleep-wake percentages were not different between the Laser-ON and Laser-OFF days. Mice failed to arouse during the 30 sec trial about 80% of the time in both treatment groups, essentially the same as spontaneous waking, indicating that the apparatus for switching the atmosphere in the plethysmography chamber did not awaken the mice.

Cortical arousal to acoustic stimuli and vibrations—As described previously (Kaur et al., 2013), we also measured the arousal response of animals to 10s of a 4 kHz acoustic stimulus of 2, 5, 10 or 30dB during the Laser-ON protocol (laser on 20 sec before and 30 sec after the acoustic stimulus) and compared that to the Laser-OFF days. Threshold sound stimuli of 2dB and 5dB failed to evoke cortical arousal in 40 and 20 % of the trials respectively (Fig. 3F and G) in both Laser-ON and Laser-OFF conditions. These responses were measured in mice (n=6) where we observed delayed arousals to CO2 upon laser inhibition as shown in Fig. 2I–L. In spite of higher latencies of arousal to CO2 with the Laser-ON the latency of the responses of the animals to the acoustic stimulus were not significantly different (Fig. 3D–G) on Laser-ON vs Laser-OFF days. Additionally, we also tested the arousal response to placing the animals (n=3) on an orbital shaker at speeds from 10 to 75 rpm. We found no difference in the arousal threshold or latency to this somatosensory and vestibular stimulation in the Laser-ON vs Laser-OFF (Fig. S5) conditions.

Experiment 3 (Inhibition of input by PBel^{CGRP} neurons to their terminal fields)

To determine which of the targets of PBel^{CGRP} neurons cause the awakening to elevated CO2; we selectively silenced terminals of the PBel^{CGRP} neurons optogenetically using ArchT. CGRP-Cre ER mice (n=32) were injected bilaterally in the PBel with AAV-FLEX-ArchT-GFP. Mice injected with AAV-FLEX-GFP served as controls (n=9). The terminal

fields selected included 3 major forebrain arousal nodes: the substantia innominata just ventral to the rostral pole of the globus pallidus in the basal forebrain (BF); the central nucleus of the amygdala (CeA); and the lateral hypothalamus (LH) at the level of the orexin neurons. We placed a unilateral glass fiber just above one of these three fields to silence $PBel^{CGRP}$ terminals on one side of the brain in each mouse, and placed a cell-specific lesion in the homologous terminal field on the other side of the brain using either ibotenic acid or an AAV-DTA. The cell body specific nature of the lesion was verified by the preservation of ArchT-GFP immunoreactive terminals in a field of gliosis and loss of neuronal cell bodies. These mice were recorded for arousal responses to 30s periods of hypercapnia in both the Laser-OFF and Laser-ON conditions.

BF—Out of 11 mice injected with AAV-Flex-ArchT-GFP in the PBel (Fig. 4A), 7 of them showed contralateral cell deletions induced by AAV-DTA, that included the projection areas of the PBel in the BF (substantia innominate and nucleus basalis) and the optical fiber accurately targeting the homologous area in the contralateral hemisphere (Fig. 4B, C–F). The lesions (left) and the terminal fields (right) in these mice were plotted and are shown as a heat map in Fig. 4B. In the Laser-OFF condition these mice had an arousal latency of 17.3 ± 0.2s to 30s of the CO2 exposure. However in the Laser-ON condition, they showed a near tripling (2.97-fold) in arousal latency (51.4 ± 2.6 s; compared to the ArchT-BF laser OFF and GFP mice- $F_{4, 18}$= 66.9; P< 0.001) (Fig. 4G–I), and they failed to arouse during the 30s of CO2 stimulation in 50.0± 6.8% of trials, which was significantly higher than both the GFP-control and the ArchT-BF Laser OFF groups ($F_{4, 18}$= 16.25; P< 0.001) (Fig. 4H &I). The latency of arousal to CO2 in the control groups, BF-GFP group and the anatomical BF-controls (n=4) with no ArchT in the terminal field, both during Laser-ON and Laser-OFF, was not different from the ArchT-BF Laser-OFF condition.

CeA—Out of 12 mice in which the CeA was targeted (Fig. 5A), 6 of them had ibotenate-induced unilateral cell deletion of the left CeA and correct placement of the glass fiber targeting the $PBel^{CGRP}$ terminal field in the right CeA (Fig. 5B) as determined by ArchT-GFP immunohistochemistry (Fig. 5C–F). Both the lesions (left) and terminal fields (right) were plotted for these 6 mice and are shown as a heat map in Fig. 5B. These mice had arousal latencies averaging 17.3 ± 1.5s to 30s of the CO2 exposure in the absence of laser inhibition (n=6), and they awakened during the 30s CO2 exposure (Fig. 5G–I) in all trials. However, in the Laser-ON condition (n=6) the arousal latency was significantly ($F_{5, 23}$= 31.27; P<0.001) increased 2.65-fold to 44.9 ± 3.5s, and in 38.2 ± 7.3% of the trials ($F_{5, 23}$= 5.38; P=0.002) there was failure to arouse during the 30s CO2 stimulus (Fig. 5G–I). By contrast, in the control group with AAV-GFP injections in the PBel (n=3), the latency to arousal during hypercapnia was not different between the Laser-ON and Laser-OFF conditions (Fig. 5G–I) and was very similar to that in the ArchT-CeA Laser-OFF group. The mice (n=6) in which the glass fiber was off target or in which there was no ArchT seen in the terminal fields served as an anatomical control group with arousal latency during the Laser-ON condition (19.3 ± 2.4 s) not significantly different from the ArchT-CeA Laser-OFF control group (Fig. 5G–I).

LH—Out of 9 mice injected with AAV-Flex-ArchT-GFP in the PBel (Fig. 6A), 5 of them showed AAV-DTA induced unilateral cell deletions in the left LH and correct placement of optical fiber that illuminated the LH terminal field on the contralateral side of the brain (Fig. 6B–F). These mice had an arousal latency of 19.7 ± 0.42 s to 30s of the CO2 exposure in the Laser-OFF condition, but in the Laser-ON condition showed a 1.65-fold increase in arousal latency to 31.7 ± 4.3 s ($F_{4, 17}$= 7.98; P= 0.010; Fig. 6G). In 27.6 ± 3.9% of the trials in the Laser-ON condition, the mouse failed to arouse during the 30s CO2 stimulus, which was significantly higher than Laser-OFF ($F_{4, 17}$= 11.01; P= 0.004; Fig. 6H&I). In mice (n=4) with no ArchT in the LH terminal fields and in the group injected with GFP (n=4), the laser inhibition did not increase the latency of arousal (18.2 ± 1.7 s and 15.5 ± 0.6 s) to CO2 and it was very similar to LH-ArchT Laser-OFF condition.

Discussion

Our results indicate that acute activation of $PBel^{CGRP}$ neurons during the normal sleep period in mice produced rapid and sustained wakefulness for 2h. However, these neurons appear to have little effect on baseline wake-sleep behavior in the absence of CO2 stimulation, because their inhibition during normocapnic trials did not change the normal duration of NREM bouts or latency to awakening. On the other hand, silencing the $PBel^{CGRP}$ cell bodies with ArchT during NREM sleep increased the mean latency to arousal to CO2 by almost four-fold, and animals failed to arouse during the stimulus at all in over half of the trials. This profound loss of sensitivity to CO2 arousal is similar to that seen in our previous work when we either ablated all of the cells in the PBel region or deleted their ability to produce the vesicular glutamate 2 transporter (Vglut2, thereby making them incapable of releasing glutamate from their terminals) (Kaur et al., 2013). Thus, the $PBel^{CGRP}$ neurons, by themselves, account for the entire CO2 arousal response from the PBel region, and ArchT silencing of those neurons is sufficient to completely abrogate that response.

To better understand the circuit basis for this response, we then used ArchT to inhibit the terminals of the PBel neurons in major forebrain terminal fields where target neurons are likely to contribute to CO2 arousal responses. We found that inhibiting $PBel^{CGRP}$ terminals in the BF had the most potent effect, achieving about 64% of the prolongation of the mean latency to arousal seen with inhibiting the CGRP cell bodies (34.1 vs 53.2 sec) and replicating the frequency of trials with failure to arouse during the 30 sec CO2 stimulus (50.0% vs 49.8%) (Fig. 7). Given the fact that the terminal field is irregular in shape and not every CGRP cell in the PBel may express ArchT, this result indicates that the bulk of the arousal effect from the CGRP-PBel neurons depends upon the relay in the BF. This result would be consistent with recent findings that BF neurons are necessary for maintaining a waking state (Fuller et al., 2011) and that the BF contains GABAergic neurons that can drive wakefulness, as well as glutamatergic and cholinergic neurons that promote cortical EEG frequencies associated with wakefulness (Anaclet et al., 2015;Xu et al., 2015).

Inhibition of $PBel^{CGRP}$ terminals in the CeA had the next most potent effect. This delayed the mean time to arousal by 28.0 sec, about 53% of the latency seen with inhibition of the cell bodies, and had about 75% of the impact on failure to arouse (38.2%). However, the

CeA is the most compact of the PBel targets, and the easiest to lesion or cover with laser light completely. In addition, the CeA does not project directly to the cerebral cortex but rather projects heavily to the BF and LH (Gastard et al., 2002;Jolkkonen et al., 2001). Hence it appears likely that the CeA is an important part of the network of $PBel^{CGRP}$ targets that causes arousal, but that it probably participates mainly by relaying and perhaps amplifying the signal to the BF and LH.

Inhibition of $PBel^{CGRP}$ terminals in the LH had the least potent effect on CO2 arousal, producing about 23% of the effect of inhibiting the $PBel^{CGRP}$ cell bodies, as measured by delaying the latency to arousal (12.0 vs. 53.2 sec), and about 55 % of the impact on failure to arouse during the CO2 stimulus (27.6% of trials). The $PBel^{CGRP}$ terminal field in the LH is also large and diffuse, so this is likely to represent a lower bound estimate of its role in CO2 arousal. LH neurons that drive arousal include orexin neurons that directly activate cerebral cortex, as well as GABAergic neurons that inhibit the sleep system (Lee et al., 2005;Venner et al., 2016). Thus it seems likely that CGRP inputs to these cell groups play a role in the arousal caused by $PBel^{CGRP}$ neurons, but probably are less potent than those in the BF.

A model for the interactions of these regions in producing arousal with visceral stimuli, including hypercapnia, is shown in Fig. 8.

Technical considerations

The method we used for simulating hypercapnia during an obstructive apnea is designed to produce a CO2 stimulus of about the duration and intensity of one encountered in sleep apnea (Kaur et al., 2013). In this model, we switch from room air to 10% CO2 in the gas entering the plethysmograph at the onset of the 30 sec stimulus. As shown in fig. 3, this causes a geometric increase in CO2, asymptotically approaching 10% by about 10 sec into the stimulus period. Intact animals typically arouse between 15 and 20 sec after stimulus onset, and in nearly all cases by 30 sec. Animals typically arouse briefly (for a few seconds) and immediately go back to sleep once the CO2 levels fall; the trials are separated by 5 min, and mice appear to recover to baseline between trials because there is little change in latency to arousal across the two hour test period. Because we run these studies during the first part of the light period, when mice are mainly sleeping, most of these trials start during NREM sleep. We analyze the trials in which the animal is soundly in NREM sleep (at least for 30 sec prior to stimulus onset). As animals spend about ten-fold more time in NREM than REM sleep, and REM bouts are shorter, only a few of our CO2 stimuli fall during REM bouts, and we therefore do not have enough data on them to analyze statistically. It is also important to recognize that mean NREM bout length extending across normocapnic gas exchange trials is about 149 sec, so that the mean time to arousal for mice that have already been in NREM for an average of 57 sec is about 92 sec, even if the animals are left undisturbed. Thus, when inhibition of the $PBel^{CGRP}$ cell bodies delays mean time to arousal to 70 sec, it is almost eliminating the CO2 arousal response entirely.

ArchT provided a very effective means for silencing $PBel^{CGRP}$ neurons in our slice preparation experiments. We used 60 sec periods of inhibition, and it can be seen in fig. 2 that in vitro, this resulted in complete silencing during the ArchT activation, but then a rebound increase in firing lasting 1–2 minutes after the silencing ended. It appears that this

protocol can be safely used to inhibit PBel^{CGRP} neurons repeatedly with an interval of 5 min between inhibition trials, because there was no histological damage to the brain after laser exposure and because the animals had normal CO2 arousal during Laser-OFF trials performed after Laser-ON trials. ArchT has been used to silence neurons in vivo in a wide variety of recent studies (Boada et al., 2014;Campos et al., 2016;Daou et al., 2016;Kim et al., 2015;Shi et al., 2015;Stefanik et al., 2013;Stefanik and Kalivas, 2013;Tsunematsu et al., 2013), and this use has also been validated by extracellular recordings from neocortical areas (Chow et al., 2010;Chuong et al., 2014). It has recently been reported that ArchT activation may excite some terminals (Mahn et al., 2016) instead of inhibiting them, but that is unlikely to be the case in these experiments, as the results of using ArchT to inhibit the PBel^{CGRP} terminals in the forebrain were very similar to those for using ArchT to inhibit the CGRP cell bodies in the PBel, and both were similar to the results of deleting Vglut2 from PBel CGRP neurons, or ablating them genetically (Kaur et al., 2013).

Mechanisms of arousal from apnea

During apnea, there is a gradual increase in blood CO2 and fall in O2. Blood O2 tension is measured by chemoreceptors in the carotid body, which are innervated by the carotid sinus branch of the glossopharyngeal nerve (Gonzalez et al., 2010;Izumizaki et al., 2004). Afferents from the carotid sinus nerve terminate in the lateral and commissural parts of the NTS (Abbott et al., 2013;Finley and Katz, 1992;Gonzalez et al., 2003;Massari et al., 1996), and hypoxia activates neurons in the ventrolateral medulla, including the C1 neurons, as well as in the locus coeruleus and the orexin neurons in the LH, in addition to the PBel, lateral crescent, and Kolliker-Fuse nucleus (Song et al., 2010;Teppema et al., 1997). Rising CO2 is in part recognized by the carotid body chemoreceptors, but also by central chemoreceptors. The retrotrapezoid chemoreceptor neurons are necessary for normal response to hypercapnia, as shown by animals or humans that have mutations in the phox2B transcription factor and fail to develop retrotrapezoid neurons (Abbott et al., 2009;Guyenet et al., 2010;Haxhiu et al., 1996;Marion and Bradshaw, 2011;Ramanantsoa and Gallego, 2013). These individuals have central apneas particularly during sleep, due to low sensitivity to elevated CO2 (Marion and Bradshaw, 2011;Ramanantsoa and Gallego, 2013). In addition, many serotonin neurons in the brainstem raphe are also CO2-sensitive. Genetic deletion of these neurons also reduces CO2 sensitivity (waking up response during sleep), although that sensitivity can be recovered by administering a 5HT2a agonist drug (Buchanan and Richerson, 2010;Ray et al., 2011;Ray et al., 2013;Richerson et al., 2005;Smith et al., 2012). This suggests that the serotonin neurons mainly set the level of CO2 sensitivity, and that their own increase in firing in response to CO2 is not required for animals to arouse to CO2.

The reductions in CO2 sensitivity for causing arousal from NREM sleep following loss of brainstem serotonin neurons is roughly in the same range as that seen with lesions of the PBel region. However, our experiments here show that within the PBel region the arousals to CO2 are dependent almost entirely upon the PBel^{CGRP} neurons. These neurons have only ascending projections (Krukoff et al., 1993;Saper, 1982;Saper and Loewy, 1980;Yasui et al., 1989), so they are likely to be downstream both of the serotonin and retrotrapezoid effects on CO2 arousal. Also, we did not observe any change in ventilatory drive to CO2 due to photo-inhibition of the PBel^{CGRP} neurons, suggesting that silencing PBel has little if any

effect on respiratory drive during hypercapnia. This suggests that it should be possible to suppress EEG arousals during apnea, while allowing the brainstem respiratory system more time to re-open the airway. On the other hand, respiratory drive and airway re-opening was greatly enhanced in all animals almost immediately after EEG arousal, suggesting that forebrain arousal results in a descending influence that plays a critical role in rapidly re-opening the airway.

An additional source of arousing stimulation during obstructive apneas is thought to be generated by the negative upper airway pressure as the individual tries to breathe against a closed airway (Carberry et al., 2015;Eckert et al., 2007;Eckert et al., 2008;Gonzalez et al., 2003;Gonzalez et al., 2010;Horner et al., 1991). The negative airway pressure is sensed by the recurrent laryngeal and superior laryngeal branches of the vagus nerve, which terminate in the same parts of the NTS as the carotid sinus nerve (Mifflin, 1996;Song et al., 2010). These NTS neurons also project heavily to the PBel region (Jhamandas and Harris, 1992;Roman et al., 2016;Rosen et al., 2011). Thus, although our model does not include upper airway occlusion, it is likely that there is a convergence of information from all three ascending sensory pathways (hypoxia and hypercarbia, which are both blocked by PBel Vglut2 deletions; and airway mechanoreceptors) in the PBel. It will be important for future work to test this hypothesis.

Yet another possibility is that CO2 could be sensed via olfactory receptors. As we discussed in our initial paper on CO2 arousal (Kaur et al., 2013), this is quite unlikely to cause the arousal seen in our paradigm. Because peripheral CO2 receptors in the olfactory system (Hu et al., 2007) respond at levels as low as 1% CO2, one would expect that our 10% CO2 stimulus would produce almost immediate arousal. However, the latency to arousal is about 15 sec, which would be more consistent with a response to a change in blood pCO2. Even if olfactory aversive responses to CO2 were involved in our model, they would have to be conveyed through the PBel ^{CGRP}, as photo inhibition at that site blocks the arousal.

Thus the PBel provides a convergence site for the entire range of neural pathways stimulated by obstructive apnea. The PBel^{CGRP} neurons provide the main relay for these stimuli to reach forebrain sites to cause wakefulness, which in turn augments airway opening, and permits the individual to survive the apneic event. Although other brainstem cell groups may participate in CO2 responses, such as the serotonergic dorsal raphe (Buchanan and Richerson, 2010;Ray et al., 2011;Ray et al., 2013;Richerson et al., 2005;Smith et al., 2012) and noradrenergic locus coeruleus neurons (Carter et al., 2010;Gargaglioni et al., 2010;Yackle et al., 2017), they clearly cannot cause normal arousal to elevated CO2 without the PBel^{CGRP} neurons. How they participate, presumably in a modulatory role, is the subject of our current investigation.

The PBel CGRP neurons as a house alarm system

In addition to receiving stimuli during hypoxia and hypercapnia, the PBel^{CGRP} neurons also send dendrites into the ascending stream of afferents from the medial part of the nucleus of the solitary tract (which conveys a variety of gastrointestinal inputs) and from the spinal cord (which largely conveys pain afferents) (Bernard et al., 1989;Bernard et al., 1994;Bernard et al., 1995;Herbert et al., 1990;Krukoff et al., 1993;Yoshida et al., 1997). Previous work has

emphasized the PBel^{CGRP} projection to the CeA as being activated by painful stimuli (Han et al., 2015). Pain is known to reduce and fragment sleep. We hypothesize that the effect of pain on sleep may also be mediated by the PBel^{CGRP} neurons

Similarly, Palmiter and colleagues have recently proposed that during feeding, CGRP neurons in the PBel may provide an early brake on food consumption (Carter et al., 2013;Carter et al., 2015), perhaps in response to vagal inputs registering gastric stretch or other early signals of satiety (Bernard et al., 1994). Inhibition of these neurons by inputs from agouti-related peptide neurons in the hypothalamus may permit prolonged feeding (Campos et al., 2016). PB neurons have been shown to fire in a lower frequency range when stimulated by visceral stimuli, whereas they fire at higher frequency range when stimulated by cutaneous noxious stimuli (Bernard et al., 1994). Therefore, it is possible that a single population of CGRP neurons may activate different responses from its upstream targets in a frequency-dependent manner. Alternatively, different subpopulations of PBel^{CGRP} neurons may receive and process different classes of aversive stimuli. This would allow some PBel^{CGRP} neurons to be activated by spinal inputs and others by inputs from the vagus nerve via the NTS.

In our model, the CGRP neurons may be a more generalized cause of wakefulness due to visceral discomfort akin to a house alarm that can be activated by different sources of potential danger (Saper, 2016). On the other hand, understanding more about afferents that modulate the PBel^{CGRP} neurons may allow us to design interventions that prevent sleep fragmentation due to pain or sleep apnea.

STAR Methods

Animals

We used CGRP-CreER mice that were produced by Dr. Pao-Tien Chuang's laboratory (Song et al., 2012) and which had been backcrossed to the C57BL6 genotype for at least 6 generations. We validated these mice for the expression of Cre in the CGRP neurons, by crossing them with TD Tomato mice (B6; 129S6-Gt(ROSA)26Sor $^{tm9(CAG-tdTomato)Hze/J}$) and after injections of Tamoxifen (TM; Sigma-Aldrich; n=3) found a 100% co-localization of the Cre and CGRP expression in the PBel and surrounding region (Fig. 1A).

All mice used in these experiments were male. Mice were derived from heterozygote matings with wild type C57BL6 mice, producing CGRP-CreER mice (heterozygotes) and wildtype littermates. Animals were maintained on a 12 h light/dark cycle with ad libitum access to water and food and after surgery were singly housed. Male littermates were randomly assigned to the experimental groups. All animal procedures met National Institutes of Health standards, as set forth in the Guide for the Care and Use of Laboratory Animals, and all protocols were approved by the Beth Israel Deaconess Medical Center Institutional Animal Care and Use Committee.

Tamoxifen Administration

Tamoxifen (TM; Sigma-Aldrich) was dissolved in Mazola corn oil to make a stock solution of 20 mg/ml. Mice (8–12wks) were injected intraperitoneally (i.p.) with TM (75 mg/kg body

weight) once every 24h for a total of 5 consecutive days. These injections were made just prior to the injections of AAVs in the brain.

Vectors

The adeno-associated viral vectors (AAVs) that we used contained the gene construct (FLEX-hM3Dq-mCherry-wpre) were acquired from Dr. Patrick M. Fuller who has previously used it to selectively activate cell populations in the basal forebrain in vivo (Anaclet et al., 2015). In addition, we also used an AAV conditionally expressing subunit A of diphtheria toxin in a Cre-dependent manner (AAV-lox-mCherry-lox-DTA-lox2; or AAV-Flex-DTA) in the CGRP-CreER mice. This vector was packaged into an AAV (serotype 10), was placed within a FLEX cassette. Within the FLEX cassette the DTA sequence is inverted, and as such it cannot be transcribed except in the presence of cre-recombinase, conferring absolute expression selectivity. This construct also contained mCherry, with mCherry located external to the FLEX switch. Hence mCherry was expressed in all non-cre-recombinase cells within the injection field, thereby allowing us to ascertain both the anatomic extent of the injection, and demonstrate, quantitatively, “survival” of the non-cre-recombinase cells intermingled with the cre-recombinase cells targeted by DTA. This vector was also designed, produced and validated by Drs. Patrick M. Fuller and Michael Lazarus. We tested the Cre dependent deletions of the CGRP-Cre neurons by unilateral injection of AAV-Flex-DTA in CGRP-CreER mice (n=3), that were crossed to GFP reporter mice (R26-loxSTOPlox-L10-GFP) in which all Cre containing cells produce GFP. Unilateral injection of the AAV-Flex DTA (150–200nl) in these mice killed all the Cre expressing CGRP neuron on the side of injection, which can be compared the intact uninjected side (Fig-S2, in which all of the surviving cells (non-Cre) on the injected side expressed mCherry). Beside CGRP-CreEr mice, we found similar results after testing this virus for selective the Cre-dependent deletions in various other lines such as Dopamine beta –hydroxylase- Cre (DβH-Cre) mice for deletion of the noradrenergic neurons in the locus coeruleus, and Corticotropin releasing hormone-Cre (CRH-Cre) mice for deletion of the CRH neurons in the Barrington nucleus. The third virus which we used in our optogenetic experiments is the optogenetic neural silencer AAV-CAG-FLEX-ArchT-GFP that co-expresses ArchT and GFP in a Cre dependent manner. This viral vector was procured from the University of North Carolina (UNC) vector core and has been used previously by many groups for silencing neurons and of their terminals (Herrera et al., 2016;Kim et al., 2015;Stefanik and Kalivas, 2013). In order to test the Cre dependent expression of the silencer AAV-CAG-FLEX-ArchT-GFP, we injected this in to PBel of mice that were heterozygous both for the CGRP-CreER and TD Tomato alleles (n=3). In these mice, all Cre-expressing neurons were labeled by Tomato red. We found expression of ArchT (as shown by GFP) only in Cre expressing CGRP cells (Fig. S3 and this figure relate to Fig 2 in the main text).

Generation of AAV

The detailed process for the generation of the AAV-FLEX-hM3Dq-mCherry-wpre has been described earlier in vivo (Anaclet et al., 2015). For the packaging of AAV-FLEX-DTA, AAV of serotype rh10 were generated by tripartite transfection (AAV-rep2/caprh10 expression plasmid, adenovirus helper plasmid, and pAAV plasmid) into 293A cells. After 3 d, the 293A cells were resuspended in artificial CSF, freeze-thawed four times, and treated with

benzonase nuclease (Millipore, Billerica, MA) to degrade all forms of non-viral DNA and RNA. Subsequently, the cell debris was removed by centrifugation and the virus titer in the supernatant was determined with an AAVpro Titration Kit for Real Time PCR (Takara, Japan). The third virus vector AAV-CAG-FLEX-ArchT-GFP was packaged at the UNC vector core.

Surgery

Experiment 1 (Activation of CGRP-PBel neurons)—In the first set of experiments, after treating CGRP-Cre ER mice for five days with TM, we sterotaxically injected 150–200nl of a solution containing AAV-hSyn-Flex-hM3Dq-mCherry-wpre in the lateral PB bilaterally (n= 6; Fig. 1B&C) and later implanted the mice for EEG and EMG recording. Five weeks after the injection of the viral vectors (to allow for Cre recombination and gene expression), these mice were attached via cables to the sleep recording apparatus. After 3–4 days of habituation to the cables and recording apparatus, sleep was recorded for 24h after injection of either saline or clozapine-N-oxide (CNO) at two different doses (0.1mg/kg or 0.3mg/kg). Mice were injected with saline or CNO at 8am (an hour after beginning of the light phase).

Optogenetic activation of the PBel^{CGRP} neurons: CGRP-Cre ER mice after injections of TM were sterotaxically injected with 150–200nl of AAV-EF1a-DIO-hChR2-EYFP (ChR2; n=6) or AAV-GFP (GFP; n=3) in the lateral PB bilaterally (n= 6; Fig. S1) and later implanted with EEG and EMG and glass fibers targeting the PB bilaterally. Five weeks after the injection of the viral vectors, these mice were attached via cables to the sleep recording apparatus. After 3–4 days of habituation to the cables and recording apparatus, sleep was recorded for 24h with and without laser stimulations. All mice were subjected to blue laser (473 nm) pulses for 5 sec every 5 minutes during the light phase. The response of laser pulses (10 ms) of three different frequencies of 5Hz, 10Hz and 20Hz were tested for producing cortical arousal when the mouse was asleep in the early light phase starting at 9 am and lasting until 2pm. Optogenetic induced wakefulness shown in Fig. S1 relates to Fig. 1 in the main text.

Experiment 2 (Inhibition of CGRP-PBel neurons)—To conduct optogenetic inhibition of CGRP PBel neurons, CGRP-Cre ER mice (n=16) were injected on one side of the brain with either an adeno-associated viral vector containing the gene for archaerhodopsin T TP009 (ArchT; n=12; 150–200nl) in a Cre-inducible FLEX cassette (AAV-FLEX-ArchT-GFP) that expressed ArchT in CGRP positive PBel cells; or an AAV–FLEX-GFP virus vector (n=4). On the other side of the brain in all 16 mice, we deleted the CGRP neurons by injecting a Cre dependent virus expressing the diphtheria toxin subunit A in a Cre-dependent manner (AAV-FLEX-DTA; volume- 150–200nl. An addition set of control mice (wildtype litter mates of CGRP-CreER; n=6) were also injected with AAV-FLEX-ArchT-GFP on left side and AAV-FLEX-DTA on the other side. This served as control group both for the Cre dependent expression of ArchT and the effect of the laser light on behavior. Mice were also instrumented for sleep recording and received unilateral surgical implantation of a Mono optic fiber (Doric Lenses, Quebec, QC, Canada), above the PB (AP, −5.3 mm; ML, 1.3 mm; DV, 2.8 mm).

Experiment 3 (Inhibition of CGRP-PBel input to forebrain terminal fields)—To conduct optogenetic inhibition of the terminal fields of the CGRP-PBel neurons, CGRP-Cre ER mice (n=32) were injected bilaterally with AAV-FLEX-ArchT-GFP (volume- 150–200nl); and another set of CGRP-Cre ER mice (n= 12) were injected with AAV–FLEX-GFP as a control group. In each of these mice, one terminal field of CGRP-PBel neurons was lesioned, including either the central nucleus of the amygdala (CeA; AP, 1.2 mm; ML, 4.8 mm; DV, 2.4 mm); the substantia innominata in the basal forebrain (BF; AP, 0.15 mm; ML, 2.4 mm; DV, 4.0 mm); or the lateral hypothalamus (LH; AP, 1.4 mm; ML, 4.5 mm; DV, 1.5 mm). Lesions were made by injecting these sites unilaterally (left side) with either 3% Ibotenic acid (n=15; volume-20–25nl) or a combination of AAV-Cre-GFP + AAV-Flex-DTA (1:1; n=29; 25nl) that caused unilateral cell deletion in the injected areas. Neuronal deletions were confirmed histologically by Nissl's staining post-hoc. After injections, all these mice were also implanted for EEG/EMG and received an optic fiber on the side of the brain opposite the lesion (right) targeting the homologous site.

Data acquisition

Five weeks after injection of the viral vectors, mice were attached to the recording cables and acclimatized to the recording chamber for 2 days. Experiment 1: EEG/EMG were recorded for 24 h after injection at 9 am of either saline or clozapine-N-oxide (CNO) at one of two different doses (0.1mg/kg or 0.3mg/kg) in randomized order, with different treatments separated by a gap of seven days. Sleep recordings were done using a preamplifier connected to a data acquisition system (8200-K1-SE) and Sirenia Software (from Pinnacle Technology). For optogenetic activation experiments, animals were also habituated for 3–4 days to the cables and recording apparatus and then sleep was recorded for 24h with and without laser stimulations (Fig. S1). Experiments 2 and 3: Mice were connected to cables both for sleep recording as well as for transmitting laser light through the pre-implanted glass fiber, and were placed in the plethysmographic chamber beginning at 9:00 A.M. for 3–4 h on each test day. They also then received one of the following protocols in a random order. Each of these protocols were repeated for each mouse for two days; on one of the days the laser was switched on (Laser-ON) and on the other day the laser was off (Laser-OFF), again in random order. On the Laser-ON protocol, a 593nm laser was ON for 60s followed by 5 mins off, and this was repeated 20 times per session. In the Laser-OFF condition, everything was the same, except that the laser light was not turned on. Twenty seconds after the scheduled onset of the laser, the gas intake for the plethysmograph was switched either to normocapnic air (21% O2, 79% N2) or hypercapnic air (10% CO2, 21% O2, and 69% N2) for 30 sec. In some trials with normocapnic air, an acoustic tone (4 kHz ranging from 2 to 30 dB) was presented for 10 s beginning 20 sec after laser onset, at 300 s intervals, with each tone presented 10–12 times, in ascending order of intensity. Arousal threshold was also tested using an orbital shaker with stimulus ranging from 10 rpm to 75 rpm (with plethysmographs placed on the orbital shaker) presented for 10 s in a similar way as the acoustic stimulus in ascending order of intensity (Fig. S5). For the normocapnic, hypercapnic, acoustic stimuli and vibrations stimulus, trials were analyzed for latency to arousal only for those epochs where the mouse was in NREM sleep for at least 30 s before the stimulus onset.

All recordings during CO2 stimulation were done in a plethysmographic chamber (unrestrained whole-body plethysmograph, Buxco Research Systems) allowing us to record the breathing of the mouse while in the chamber. Electroencephalogram (EEG) and electromyogram (EMG) were recorded using Pinnacle preamp cables connected to the analog adaptor (8242, Pinnacle Technology). Gas levels in the chamber were continuously monitored using CO2 and O2 monitors from CWE, Inc (Ardmore, PA, USA). EEG, EMG, respiration, and CO2 and O2 levels were fed into an Axon Digidata 1322A analog-to-digital converter and the signals were acquired using Axoscope software (Molecular Devices, Foster City, CA, USA). Respiratory data was analyzed as per the method in data analysis section and results shown in Fig. S4.

Laser light: Mice were allowed at least 2 d to acclimate to fiberoptic cables (1.5 m long, 200 μm diameter; Doric Lenses, Quebec, QC, Canada) and connecting interfaces coated with opaque heat-shrink tubing before the experimental sessions. During Laser-ON experiments, light pulses were programmed using a waveform generator (Agilent Technologies, catalog #33220A, CA, USA) to drive an orange-yellow light laser (593 nm; Laser Glow, Toronto, ON, Canada) to be on for 60s beginning 20 s before the onset of the CO2 (or air or acoustic) stimulus. We adjusted the laser such that the light power exiting the fiber-optic cable was 8–10 mW, and this was checked before and after the experiment. Using an online light transmission calculator for brain tissue (www.stanford.edu/group/dlab/cgi-bin/graph/chart.php), we estimated the light power at the PBel to be less than10 mW/mm^2 and a similar range has been used by most researchers for neuronal silencing at the terminal fields (Herrera et al., 2016;Kim et al., 2015;Stefanik and Kalivas, 2013). Note that this is probably a high estimate because some light is probably lost at the interface between the fiber-optic cable and the implanted optic-fiber.

Data analysis

Sleep analysis—Digitized polygraphic data were analyzed off-line in 10 s epochs using Sleep Sign software (Kissei Comtec Co. Ltd., Matsumoto, Nagano, Japan). The software autoscored each epoch using an algorithm that identified three behavioral states based on EEG and EMG. The autoscored data were then checked at least twice visually for movement and any other artifact and to confirm or correct automatic state classification by an unbiased scorer blind to the treatment groups (JW). Over-reading of the sleep recordings were done according to previously published criteria (Neckelmann and Ursin, 1993; Kaur et al., 2008). The changes in amount of time spent in wake, non-rapid-eye-movement (NREM) sleep, and rapid-eye-movement (REM) sleep in different treatment groups (saline vs. CNO 0.1 and 0.3 mg/kg) across time and over light and dark phases were compared statistically using a two-way ANOVA followed by a Holm-Sidak post hoc test for multiple comparisons. Similarly, for experiments 2 and 3, the percentage of time spent in NREM, wake and REM sleep during the Laser-ON and Laser-OFF days was statistically compared to the normocapnic air condition. In order to see if the Laser-ON condition directly affected sleep maintenance or promoted sleep, sleep to wake transitions during the 60s Laser-ON were compared with similar 60s period during the laser-OFF day.

Statistical analysis—All statistical analyses were performed using SigmaPlot 12.3 (Systat Software, Inc.). For statistical comparisons, we first confirmed if the data meets with the assumptions of the ANOVA, then either one way or two way ANOVA was performed to compare the effects between various treatment groups during the light and dark phase. If differences in the mean values among the treatment groups were greater than would be expected by chance; then all pairwise multiple comparisons were performed using the Holm-Sidak method. The F and P values are described in the results section with details of the statistical tests also given in the respective figure legends and represented in figures. The 'n' in the figures and results represents the number of animals. We also used the same software to test the sample size and power of the tests post hoc and experiments were found to be sufficiently powered. A probability of error of less than 0.05 was considered significant.

Analysis of arousal to hypercapnia—EEG arousals in response to stimuli were identified by EEG transition from NREM to a waking state, which was usually accompanied by EMG activation, as described previously (Kaur et al., 2013). We scored the duration and latency of all the EEG arousals that occurred after onset of stimulation. The trials in which animals did not awaken during the 30 s of the CO2 or air stimulus were marked as failure to arouse to stimulus. These arousals were compared across the Laser-ON and Laser-OFF days.

Analysis of the ventilatory kinetics during hypercapnia—Respiratory airflow was recorded using the plethysmograph chamber (Data Science International, St. Paul, MN) attached to flow transducers connected to an A/D board that transmitted signals to the computer. Volume calibrations for these chambers were performed by repeated known volume air injections. Flow transducer readings were digitized at 1 kHz and recorded using Axoscope software (Molecular Devices, Foster City, CA, USA). The flow signals were analyzed offline for respiratory rate, tidal volume, and ventilation using software to automatically detect the peaks and troughs of each breath (Matlab, Mathworks Inc., Natick, MA). Trials for a particular condition (with and without Laser-ON) were ensemble averaged. We then compared the respiratory variables for three breaths before hypercapnia to that during hypercapnia just prior to waking in response to CO2 (shown in Fig. S4; respiratory data shown relates to Fig. 2 in the main text).

Histology—At the conclusion of the experiment, the animals were perfused with 0.9% saline followed by 10% buffered formalin while under deep anesthesia. Brains were harvested for analysis of the effective location of the injection site. Brains were kept in 30% sucrose for 2 d and sections were cut at 30μm using a freezing microtome in four 1:4 series.

Immunohistochemistry—One of the series of sections was immunostained for either GFP (Rabbit anti-GFP, 1:10K, ThermoFisher Scientific, Cat- A11122) or mCherry (anti dsRed, 1:10k, Cat-632496, Clontech) using standard immunohistochemistry protocols described previously (Kaur et al., 2013). Neither of these antibodies stained tissue from control mice that were not injected with viral vectors. Another series was double-stained for immunofluorescence either with antibodies for GFP using mouse anti-GFP or dsRed and also stained with CGRP antibody (Rabbit-anti-CGRP, 1:1000, T-4032, Peninsula Laboratories International Inc.). The CGRP antibody stained a pattern of neurons in the

parabrachial region, hypothalamus, basal forebrain, and amygdala, as previously reported (Yasui et al., 1989) and there was nearly perfect correspondence between immunostaining and Cre-dependent fluorescent protein expression in CGRP-CreER mice (see below). No immunostaining was seen when the primary antibodies were omitted. Sections for immunostaining were first incubated in 0.1 M phosphate buffer and 1% H2O2 for 5–10 min followed by three washings in 0.1 M phosphate buffer. For all the immunohistochemical staining that involved visualization using a diaminobenzidine (DAB) reaction, the sections after the overnight incubation with primary antiserum were incubated in the respective secondary antibodies for 2 h, followed by incubation in ABC reagents (1:1000; Vector Laboratories) for 90 min, then washed again and incubated in a 0.06% solution of 3,3-diaminobenzidine tetrahydrochloride (Sigma-Aldrich) and 0.05% CoCl2 and 0.01% NiSO4 (NH4) in PBS plus 0.02% H2O2 for 5 min. Finally, the sections were mounted on slides, dehydrated, cleared, and cover-slipped. Sections for double or triple-immunofluorescence staining for GFP and dsRED or CGRP were incubated in fluorescent-labeled secondary antibodies (Pacific Blue; Alexa- 488; Alexa- 555; Molecular probes, Thermo-Fischer Scientific) for 2 h and cover-slipped with fluorescence mounting media (Dako, North America).

Histological analysis—To analyze the non-selective unilateral cell lesions and sites of terminal inhibition in the experiment 3; and define the projections areas (CeA; BF and LH) of CGRP-PBel neurons, whose inhibition prolonged the latencies to waking up in response to CO2, we plotted the lesion areas and fibers in the terminal field as heat maps and correlated them to the physiological responses (ratio of the arousal latency of each experimental mouse compared to the baseline group) of the mice. For the generation of the heat maps, each experimental mouse was given an arousal latency score based on ratio of the arousal latency compared to the baseline group. The lesion site showing extent of lesioned area on the left side and the terminal fields on the right side along with tips of the optical fibers, were mapped onto the representative templates at four rostral-caudal levels throughout CeA, BF and LH areas. These were constructed using a series of Nissl stained sections that were also immunolabelled for GFP to mark the terminal fields of PBel. The part of each mouse's terminal field that was within 1 mm of the tip of the optical fiber was weighted by its arousal latency score, and all mice were overlaid using a custom script (www.python.org) over the group that was summed (pixel by pixel over each overlaid image) and heat maps were created demarcating brain regions most associated with the increased arousal latency.

Whole cell patch clamp in vitro experiments—For *in vitro* electrophysiological recordings we used 4 CGRP-CreER mice. We injected 150nl of AAV-FLEX-ArchT-GFP (n = 3) or 150 nl of AAV-FLEX-GFP (n = 1; control experiments) into the PB bilaterally using the coordinates described above. Four weeks after AAV injections, we prepared brainstem slices for electrophysiological recordings. We deeply anesthetized the mice with isoflurane via inhalation and transcardially perfused them with ice-cold cutting ACSF (*N*-methyl-D-glucamine, NMDG-based solution) containing (in mM): 100 NMDG, 2.5 KCl, 1.24 NaH_2PO_4, 30 $NaHCO_3$, 25 glucose, 20 HEPES, 2 thiourea, 5 Na-L-ascorbate, 3 Na-pyruvate, 0.5 $CaCl_2$, 10 $MgSO_4$ (pH 7.3 with HCl when carbogenated with 95% O_2 and 5%

CO_2). We quickly removed the mouse brains and sectioned them in coronal slices (250 μm thick) in ice-cold cutting ACSF using a vibrating microtome (VT1000S, Leica, Bannockburn, IL, USA). We transferred the slices containing the lPB to normal ACSF containing (in mM): 120 NaCl, 2.5 KCl, 1.3 $MgCl_2$, 10 glucose, 26 $NaHCO_3$, 1.24 NaH_2PO_4, 4 $CaCl_2$, 2 thiourea, 1 Na-L-ascorbate, 3 Na-pyruvate (pH 7.4 when carbogenated with 95% O_2 and 5% CO_2, 310–320 mOsm). We recorded in the $PBel^{CGRP}$ that expressed GFP using a combination of fluorescence and infrared differential interference contrast (IR-DIC) video microscopy. For these recordings, we used a fixed stage upright microscope (BX51WI, Olympus America Inc.) equipped with a Nomarski water immersion lens (40 x/0.8 W) and IR-sensitive CCD camera (ORCA-ER, Hamamatsu, Bridgewater, NJ, USA), and we used AxioVision software (Carl Zeiss MicroImaging) to acquire real time images. We recorded in whole-cell configuration using a Multiclamp 700B amplifier (Molecular Devices, Foster City, CA, USA), a Digidata 1322A interface, and Clampex 9.0 software (Molecular Devices). We recorded in ACSF using a K-gluconate-based pipette solution containing (in mM): 120 K-gluconate, 10 KCl, 3 $MgCl_2$, 10 HEPES, 2.5 K-ATP, 0.5 Na-GTP (pH 7.2 adjusted with KOH; 280 mOsm). We photo-stimulated $PBel^{CGRP}$ neurons expressing ArchT using full-field 60 s light pulses (~ 3 mW/mm^2, 1mm beam width) from a 880 mW LUXEON yellow light-emitting diode (565 nm wavelength; #M565L3; Thorlabs, Newton, NJ, USA) coupled to the epifluorescence pathway of the microscope. We analyzed the electrophysiological data using Clampfit 9.0 (Molecular Devices) and IGOR Pro 6 (WaveMetrics, Lake Oswego, OR, USA).

Data availability—The data that support the findings of this study will be made available from the corresponding author upon reasonable request.

Supplementary Material

Refer to Web version on PubMed Central for supplementary material.

Acknowledgments

We thank Quan Ha and Minh Ha for their excellent technical support, and Sathyajit Bandaru for maintaining the mouse breeding program. We are also indebted to Dr. Pao-Tien Chuang's laboratory, which produced the CGRP-CreER mice and supplied us with the breeder pairs. This research work was supported by funding from USPHS grants 2P01 HL095491 and NS085477.

Reference list

Abbott SB, DePuy SD, Nguyen T, Coates MB, Stornetta RL, Guyenet PG. Selective optogenetic activation of rostral ventrolateral medullary catecholaminergic neurons produces cardiorespiratory stimulation in conscious mice. J Neurosci. 2013; 33:3164–3177. [PubMed: 23407970]

Abbott SB, Stornetta RL, Fortuna MG, Depuy SD, West GH, Harris TE, Guyenet PG. Photostimulation of retrotrapezoid nucleus phox2b-expressing neurons in vivo produces long-lasting activation of breathing in rats. J Neurosci. 2009; 29:5806–5819. [PubMed: 19420248]

Anaclet C, Pedersen NP, Ferrari LL, Venner A, Bass CE, Arrigoni E, Fuller PM. Basal forebrain control of wakefulness and cortical rhythms. Nat Commun. 2015; 6:8744. [PubMed: 26524973]

Ayalon L, Peterson S. Functional central nervous system imaging in the investigation of obstructive sleep apnea. Curr Opin Pulm Med. 2007; 13:479–483. [PubMed: 17901752]

Benarroch EE. Brainstem respiratory control: substrates of respiratory failure of multiple system atrophy. Mov Disord. 2007; 22:155–161. [PubMed: 17133520]

Bernard JF, Alden M, Besson JM. The organization of the efferent projections from the pontine parabrachial area to the amygdaloid complex: a Phaseolus vulgaris leucoagglutinin (PHA-L) study in the rat. J Comp Neurol. 1993; 329:201–229. [PubMed: 8454730]

Bernard JF, Dallel R, Raboisson P, Villanueva L, Le BD. Organization of the efferent projections from the spinal cervical enlargement to the parabrachial area and periaqueductal gray: a PHA-L study in the rat. J Comp Neurol. 1995; 353:480–505. [PubMed: 7759612]

Bernard JF, Huang GF, Besson JM. The parabrachial area: electrophysiological evidence for an involvement in visceral nociceptive processes. J Neurophysiol. 1994; 71:1646–1660. [PubMed: 8064340]

Bernard JF, Peschanski M, Besson JM. A possible spino (trigemino)-ponto-amygdaloid pathway for pain. Neurosci Lett. 1989; 100:83–88. [PubMed: 2474780]

Berquin P, Bodineau L, Gros F, Larnicol N. Brainstem and hypothalamic areas involved in respiratory chemoreflexes: a Fos study in adult rats. Brain Res. 2000; 857:30–40. [PubMed: 10700550]

Berry RB, Gleeson K. Respiratory arousal from sleep: mechanisms and significance. Sleep. 1997; 20:654–675. [PubMed: 9351134]

Boada MD, Martin TJ, Peters CM, Hayashida K, Harris MH, Houle TT, Boyden ES, Eisenach JC, Ririe DG. Fast-conducting mechanoreceptors contribute to withdrawal behavior in normal and nerve injured rats. Pain. 2014; 155:2646–2655. [PubMed: 25267211]

Bochorishvili G, Stornetta RL, Coates MB, Guyenet PG. Pre-Botzinger complex receives glutamatergic innervation from galaninergic and other retrotrapezoid nucleus neurons. J Comp Neurol. 2012; 520:1047–1061. [PubMed: 21935944]

Bonsignore MR, Esquinas C, Barcelo A, Sanchez-de-la-Torre M, Paterno A, Duran-Cantolla J, Marin JM, Barbe F. Metabolic syndrome, insulin resistance and sleepiness in real-life obstructive sleep apnoea. Eur Respir J. 2012; 39:1136–1143. [PubMed: 22075482]

Buchanan GF, Richerson GB. Central serotonin neurons are required for arousal to CO2. Proc Natl Acad Sci U S A. 2010; 107:16354–16359. [PubMed: 20805497]

Campos CA, Bowen AJ, Schwartz MW, Palmiter RD. Parabrachial CGRP Neurons Control Meal Termination. Cell Metab. 2016; 23:811–820. [PubMed: 27166945]

Carberry JC, Hensen H, Fisher LP, Saboisky JP, Butler JE, Gandevia SC, Eckert DJ. Mechanisms contributing to the response of upper-airway muscles to changes in airway pressure. J Appl Physiol (1985). 2015; 118:1221–1228. [PubMed: 25749447]

Carter ME, Han S, Palmiter RD. Parabrachial calcitonin gene-related peptide neurons mediate conditioned taste aversion. J Neurosci. 2015; 35:4582–4586. [PubMed: 25788675]

Carter ME, Soden ME, Zweifel LS, Palmiter RD. Genetic identification of a neural circuit that suppresses appetite. Nature. 2013; 503:111–114. [PubMed: 24121436]

Carter ME, Yizhar O, Chikahisa S, Nguyen H, Adamantidis A, Nishino S, Deisseroth K, de LL. Tuning arousal with optogenetic modulation of locus coeruleus neurons. Nat Neurosci. 2010; 13:1526–1533. [PubMed: 21037585]

Chow BY, Han X, Dobry AS, Qian X, Chuong AS, Li M, Henninger MA, Belfort GM, Lin Y, Monahan PE, Boyden ES. High-performance genetically targetable optical neural silencing by light-driven proton pumps. Nature. 2010; 463:98–102. [PubMed: 20054397]

Chuong AS, Miri ML, Busskamp V, Matthews GA, Acker LC, Sorensen AT, Young A, Klapoetke NC, Henninger MA, Kodandaramaiah SB, Ogawa M, Ramanlal SB, Bandler RC, Allen BD, Forest CR, Chow BY, Han X, Lin Y, Tye KM, Roska B, Cardin JA, Boyden ES. Noninvasive optical inhibition with a red-shifted microbial rhodopsin. Nat Neurosci. 2014; 17:1123–1129. [PubMed: 24997763]

Daou I, Beaudry H, Ase AR, Wieskopf JS, Ribeiro-da-Silva A, Mogil JS, Seguela P. Optogenetic Silencing of Nav1.8-Positive Afferents Alleviates Inflammatory and Neuropathic Pain. eNeuro. 2016; 3

deLacalle S, Saper CB. Calcitonin gene-related peptide-like immunoreactivity marks putative visceral sensory pathways in human brain. Neuroscience. 2000; 100:115–130. [PubMed: 10996463]

Eckert DJ, McEvoy RD, George KE, Thomson KJ, Catcheside PG. Genioglossus reflex inhibition to upper-airway negative-pressure stimuli during wakefulness and sleep in healthy males. J Physiol. 2007; 581:1193–1205. [PubMed: 17395627]

Eckert DJ, McEvoy RD, George KE, Thomson KJ, Catcheside PG. Effects of hypoxia on genioglossus and scalene reflex responses to brief pulses of negative upper-airway pressure during wakefulness and sleep in healthy men. J Appl Physiol (1985). 2008; 104:1426–1435. [PubMed: 18292297]

Finley JC, Katz DM. The central organization of carotid body afferent projections to the brainstem of the rat. Brain Res. 1992; 572:108–116. [PubMed: 1611506]

Fuller P, Sherman D, Pedersen NP, Saper CB, Lu J. Reassessment of the structural basis of the ascending arousal system. J Comp Neurol. 2011; 519:933–956. [PubMed: 21280045]

Gargaglioni LH, Hartzler LK, Putnam RW. The locus coeruleus and central chemosensitivity. Respir Physiol Neurobiol. 2010; 173:264–273. [PubMed: 20435170]

Gastard M, Jensen SL, Martin JR III, Williams EA, Zahm DS. The caudal sublenticular region/anterior amygdaloid area is the only part of the rat forebrain and mesopontine tegmentum occupied by magnocellular cholinergic neurons that receives outputs from the central division of extended amygdala. Brain Res. 2002; 957:207–222. [PubMed: 12445963]

Gonzalez C, Agapito MT, Rocher A, Gomez-Nino A, Rigual R, Castaneda J, Conde SV, Obeso A. A revisit to O2 sensing and transduction in the carotid body chemoreceptors in the context of reactive oxygen species biology. Respir Physiol Neurobiol. 2010; 174:317–330. [PubMed: 20833275]

Gonzalez C, Rocher A, Zapata P. Arterial chemoreceptors: cellular and molecular mechanisms in the adaptative and homeostatic function of the carotid body. Rev Neurol. 2003; 36:239–254. [PubMed: 12599155]

Guyenet PG, Stornetta RL, Abbott SB, Depuy SD, Fortuna MG, Kanbar R. Central CO2 chemoreception and integrated neural mechanisms of cardiovascular and respiratory control. J Appl Physiol. 2010; 108:995–1002. [PubMed: 20075262]

Han S, Soleiman MT, Soden ME, Zweifel LS, Palmiter RD. Elucidating an Affective Pain Circuit that Creates a Threat Memory. Cell. 2015; 162:363–374. [PubMed: 26186190]

Haxhiu MA, Yung K, Erokwu B, Cherniack NS. CO2-induced c-fos expression in the CNS catecholaminergic neurons. Respir Physiol. 1996; 105:35–45. [PubMed: 8897649]

Herbert H, Moga MM, Saper CB. Connections of the parabrachial nucleus with the nucleus of the solitary tract and the medullary reticular formation in the rat. J Comp Neurol. 1990; 293:540–580. [PubMed: 1691748]

Herrera CG, Cadavieco MC, Jego S, Ponomarenko A, Korotkova T, Adamantidis A. Hypothalamic feedforward inhibition of thalamocortical network controls arousal and consciousness. Nat Neurosci. 2016; 19:290–298. [PubMed: 26691833]

Horner RL, Innes JA, Murphy K, Guz A. Evidence for reflex upper airway dilator muscle activation by sudden negative airway pressure in man. J Physiol. 1991; 436:15–29. [PubMed: 2061830]

Hu J, Zhong C, Ding C, Chi Q, Walz A, Mombaerts P, Matsunami H, Luo M. Detection of near-atmospheric concentrations of CO2 by an olfactory subsystem in the mouse. Science. 2007; 317:953–957. [PubMed: 17702944]

Izumizaki M, Pokorski M, Homma I. Role of the carotid bodies in chemosensory ventilatory responses in the anesthetized mouse. J Appl Physiol. 2004; 97:1401–1407. [PubMed: 15194670]

Jhamandas JH, Harris KH. Influence of nucleus tractus solitarius stimulation and baroreceptor activation on rat parabrachial neurons. Brain Res Bull. 1992; 28:565–571. [PubMed: 1617439]

Jolkkonen E, Miettinen R, Pitkanen A. Projections from the amygdalo-piriform transition area to the amygdaloid complex: a PHA-l study in rat. J Comp Neurol. 2001; 432:440–465. [PubMed: 11268008]

Kalia M, Richter D. Rapidly adapting pulmonary receptor afferents: II. Fine structure and synaptic organization of central terminal processes in the nucleus of the tractus solitarius. J Comp Neurol. 1988; 274:574–594. [PubMed: 2464625]

Kaur S, Junek A, Black MA, Semba K. Effects of ibotenate and 192IgG-saporin lesions of the nucleus basalis magnocellularis/substantia innominata on spontaneous sleep and wake states and on recovery sleep after sleep deprivation in rats. J Neurosci. 2008; 28:491–504. [PubMed: 18184792]

Kaur S, Pedersen NP, Yokota S, Hur EE, Fuller PM, Lazarus M, Chamberlin NL, Saper CB. Glutamatergic signaling from the parabrachial nucleus plays a critical role in hypercapnic arousal. J Neurosci. 2013; 33:7627–7640. [PubMed: 23637157]

Kim T, Thankachan S, McKenna JT, McNally JM, Yang C, Choi JH, Chen L, Kocsis B, Deisseroth K, Strecker RE, Basheer R, Brown RE, McCarley RW. Cortically projecting basal forebrain parvalbumin neurons regulate cortical gamma band oscillations. Proc Natl Acad Sci U S A. 2015; 112:3535–3540. [PubMed: 25733878]

Krukoff TL, Harris KH, Jhamandas JH. Efferent projections from the parabrachial nucleus demonstrated with the anterograde tracer Phaseolus vulgaris leucoagglutinin. Brain Res Bull. 1993; 30:163–172. [PubMed: 7678381]

Lee MG, Hassani OK, Jones BE. Discharge of identified orexin/hypocretin neurons across the sleep-waking cycle. J Neurosci. 2005; 25:6716–6720. [PubMed: 16014733]

Mahn M, Prigge M, Ron S, Levy R, Yizhar O. Biophysical constraints of optogenetic inhibition at presynaptic terminals. Nat Neurosci. 2016; 19:554–556. [PubMed: 26950004]

Mannarino MR, Di FF, Pirro M. Obstructive sleep apnea syndrome. Eur J Intern Med. 2012; 23:586–593. [PubMed: 22939801]

Marion TL, Bradshaw WT. Congenital central hypoventilation syndrome and the PHOX2B gene mutation. Neonatal Netw. 2011; 30:397–401. [PubMed: 22052119]

Massari VJ, Shirahata M, Johnson TA, Gatti PJ. Carotid sinus nerve terminals which are tyrosine hydroxylase immunoreactive are found in the commissural nucleus of the tractus solitarius. J Neurocytol. 1996; 25:197–208. [PubMed: 8737172]

Mifflin SW. Convergent carotid sinus nerve and superior laryngeal nerve afferent inputs to neurons in the NTS. Am J Physiol. 1996; 271:R870–R880. [PubMed: 8897976]

Mizusawa A, Ogawa H, Kikuchi Y, Hida W, Shirato K. Role of the parabrachial nucleus in ventilatory responses of awake rats. J Physiol. 1995; 489(Pt 3):877–884. [PubMed: 8788951]

Moreira TS, Takakura AC, Colombari E, Guyenet PG. Central chemoreceptors and sympathetic vasomotor outflow. J Physiol. 2006; 577:369–386. [PubMed: 16901945]

Panneton WM, Loewy AD. Projections of the carotid sinus nerve to the nucleus of the solitary tract in the cat. Brain Res. 1980; 191:239–244. [PubMed: 7378754]

Ramanantsoa N, Gallego J. Congenital central hypoventilation syndrome. Respir Physiol Neurobiol. 2013; 189:272–279. [PubMed: 23692929]

Ray RS, Corcoran AE, Brust RD, Kim JC, Richerson GB, Nattie E, Dymecki SM. Impaired respiratory and body temperature control upon acute serotonergic neuron inhibition. Science. 2011; 333:637–642. [PubMed: 21798952]

Ray RS, Corcoran AE, Brust RD, Soriano LP, Nattie EE, Dymecki SM. Egr2- neurons control the adult respiratory response to hypercapnia. Brain Res. 2013; 1511:115–125. [PubMed: 23261662]

Richerson GB, Wang W, Hodges MR, Dohle CI, Diez-Sampedro A. Homing in on the specific phenotype(s) of central respiratory chemoreceptors. Exp Physiol. 2005; 90:259–266. [PubMed: 15728134]

Roman CW, Derkach VA, Palmiter RD. Genetically and functionally defined NTS to PBN brain circuits mediating anorexia. Nat Commun. 2016; 7:11905. [PubMed: 27301688]

Rosen AM, Victor JD, Di Lorenzo PM. Temporal coding of taste in the parabrachial nucleus of the pons of the rat. J Neurophysiol. 2011; 105:1889–1896. [PubMed: 21307316]

Saper CB. Reciprocal parabrachial-cortical connections in the rat. Brain Res. 1982; 242:33–40. [PubMed: 7104731]

Saper CB. The House Alarm. Cell Metab. 2016; 23:754–755. [PubMed: 27166934]

Saper CB, Loewy AD. Efferent connections of the parabrachial nucleus in the rat. Brain Res. 1980; 197:291–317. [PubMed: 7407557]

Shi YF, Han Y, Su YT, Yang JH, Yu YQ. Silencing of Cholinergic Basal Forebrain Neurons Using Archaerhodopsin Prolongs Slow-Wave Sleep in Mice. PLoS One. 2015; 10:e0130130. [PubMed: 26151909]

Smith, HR., Richerson, GB., Buchanan, GF. Activation of 5-HT$_{2A}$ receptors recovers hypercapnia-induced arousal in genetically central 5-HT neuron deficient mice. 2012 Neuroscience Meeting Planner Program# 799.07/BBB8 [; Washington, DC: Society for Neuroscience; 2012.

Song G, Xu H, Wang H, Macdonald SM, Poon CS. Hypoxia-excited neurons in NTS send axonal projections to Kolliker-Fuse/parabrachial complex in dorsolateral pons. Neuroscience. 2010

Song H, Yao E, Lin C, Gacayan R, Chen MH, Chuang PT. Functional characterization of pulmonary neuroendocrine cells in lung development, injury, and tumorigenesis. Proc Natl Acad Sci U S A. 2012; 109:17531–17536. [PubMed: 23047698]

Stefanik MT, Kalivas PW. Optogenetic dissection of basolateral amygdala projections during cue-induced reinstatement of cocaine seeking. Front Behav Neurosci. 2013; 7:213. [PubMed: 24399945]

Stefanik MT, Moussawi K, Kupchik YM, Smith KC, Miller RL, Huff ML, Deisseroth K, Kalivas PW, LaLumiere RT. Optogenetic inhibition of cocaine seeking in rats. Addict Biol. 2013; 18:50–53. [PubMed: 22823160]

Teppema LJ, Veening JG, Kranenburg A, Dahan A, Berkenbosch A, Olievier C. Expression of c-fos in the rat brainstem after exposure to hypoxia and to normoxic and hyperoxic hypercapnia. J Comp Neurol. 1997; 388:169–190. [PubMed: 9368836]

Tsunematsu T, Tabuchi S, Tanaka KF, Boyden ES, Tominaga M, Yamanaka A. Long-lasting silencing of orexin/hypocretin neurons using archaerhodopsin induces slow-wave sleep in mice. Behav Brain Res. 2013; 255:64–74. [PubMed: 23707248]

Venner A, Anaclet C, Broadhurst RY, Saper CB, Fuller PM. A Novel Population of Wake-Promoting GABAergic Neurons in the Ventral Lateral Hypothalamus. Curr Biol. 2016; 26:2137–2143. [PubMed: 27426511]

Xu M, Chung S, Zhang S, Zhong P, Ma C, Chang WC, Weissbourd B, Sakai N, Luo L, Nishino S, Dan Y. Basal forebrain circuit for sleep-wake control. Nat Neurosci. 2015; 18:1641–1647. [PubMed: 26457552]

Yackle K, Schwarz LA, Kam K, Sorokin JM, Huguenard JR, Feldman JL, Luo L, Krasnow MA. Breathing control center neurons that promote arousal in mice. Science. 2017; 355:1411–1415. [PubMed: 28360327]

Yasui Y, Saper CB, Cechetto DF. Calcitonin gene-related peptide immunoreactivity in the visceral sensory cortex, thalamus, and related pathways in the rat. J Comp Neurol. 1989; 290:487–501. [PubMed: 2613940]

Yasui Y, Saper CB, Cechetto DF. Calcitonin gene-related peptide (CGRP) immunoreactive projections from the thalamus to the striatum and amygdala in the rat. J Comp Neurol. 1991; 308:293–310. [PubMed: 1890240]

Yokota S, Kaur S, VanderHorst VG, Saper CB, Chamberlin NL. Respiratoryrelated outputs of glutamatergic, hypercapnia-responsive parabrachial neurons in mice. J Comp Neurol. 2015; 523:907–920. [PubMed: 25424719]

Yoshida A, Chen K, Moritani M, Yabuta NH, Nagase Y, Takemura M, Shigenaga Y. Organization of the descending projections from the parabrachial nucleus to the trigeminal sensory nuclear complex and spinal dorsal horn in the rat. J Comp Neurol. 1997; 383:94–111. [PubMed: 9184989]

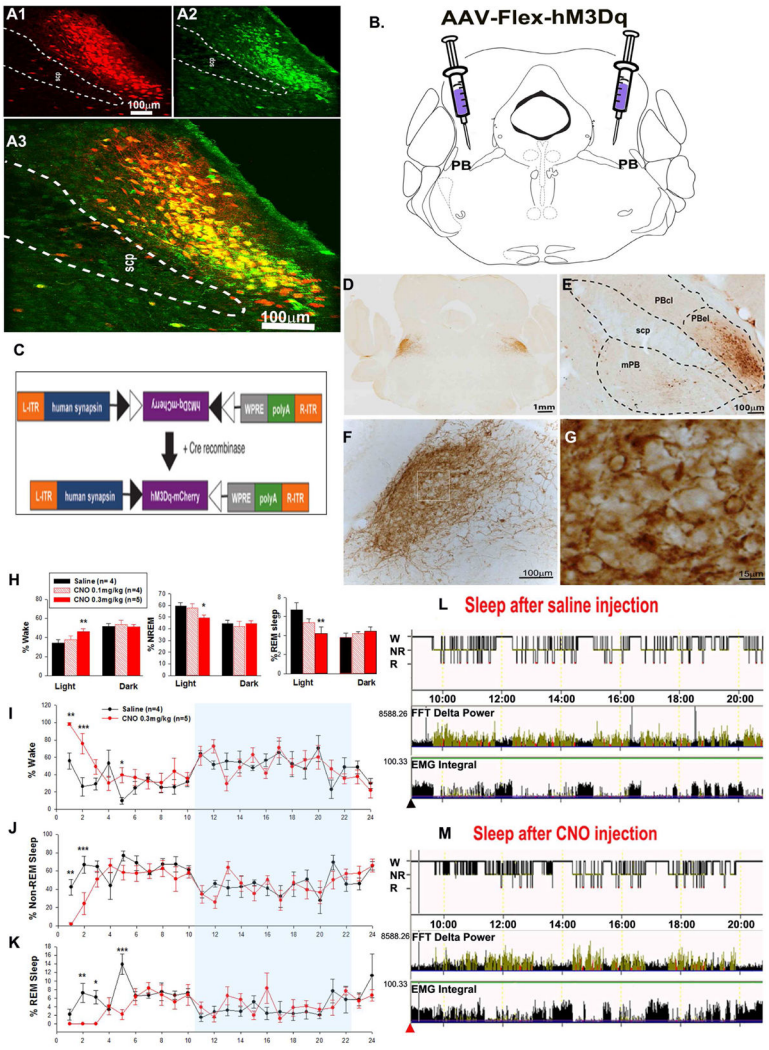

Figure 1. Chemogenetic activation of the PBel^{CGRP} neurons produces wakefulness

CGRP-Cre-ER mice were crossed with td-Tomato reporter mice, resulting in nearly all of the Cre-containing cells in the PBel (red in A1) also expressing CGRP (green in A2), as seen in the merged image (A3). B, a drawing schematically showing the experimental strategy for chemogenetic activation of PBel^{CGRP} and C the construct of the AAV-FLEX-hM3Dq-mcherry used in the study. D is a photomicrograph of coronal section of a mouse brain immunostained for mcherry (co-expressed with hM3Dq) localized to the CGRP positive neurons in the PBel. Panels E–G are further magnifications of the section shown in D (E right side, F, G left side). Panel H compares the percentage time spent in wake, non-REM and REM sleep (mean ± SEM) during the light dark phase, after either saline (black) or two different doses of CNO (0.1 mg/kg pink or 0.3mg/kg red); while hourly comparison (mean ± SEM) is shown in I-K for the 0.3 mg/kg dose. L and M are representative hypnograms from a mouse injected with saline (L) and CNO (0.3mg/kg, M) on two different days at the beginning of light phase (marked by black and red triangles). The upper trace in each panel shows time spent in wake (W), Non-Rem (NR), and REM sleep (R). The middle trace shows the delta power in the EEG, with bouts of NREM sleep shown in green, REM sleep in red,

and wake in black. The lowest trace, EMG, show periods of movement, mostly seen during wake. **Abbreviations:** PB, parabrachial nucleus, el external lateral, cl central lateral, dl dorsal lateral, m medial PB subnuclei; scp, superior cerebellar peduncle. (***- P< 0.001, **- P<0.01 and *- P<0.05, 2-way ANOVA followed by Holm-Sidak for multiple comparison).

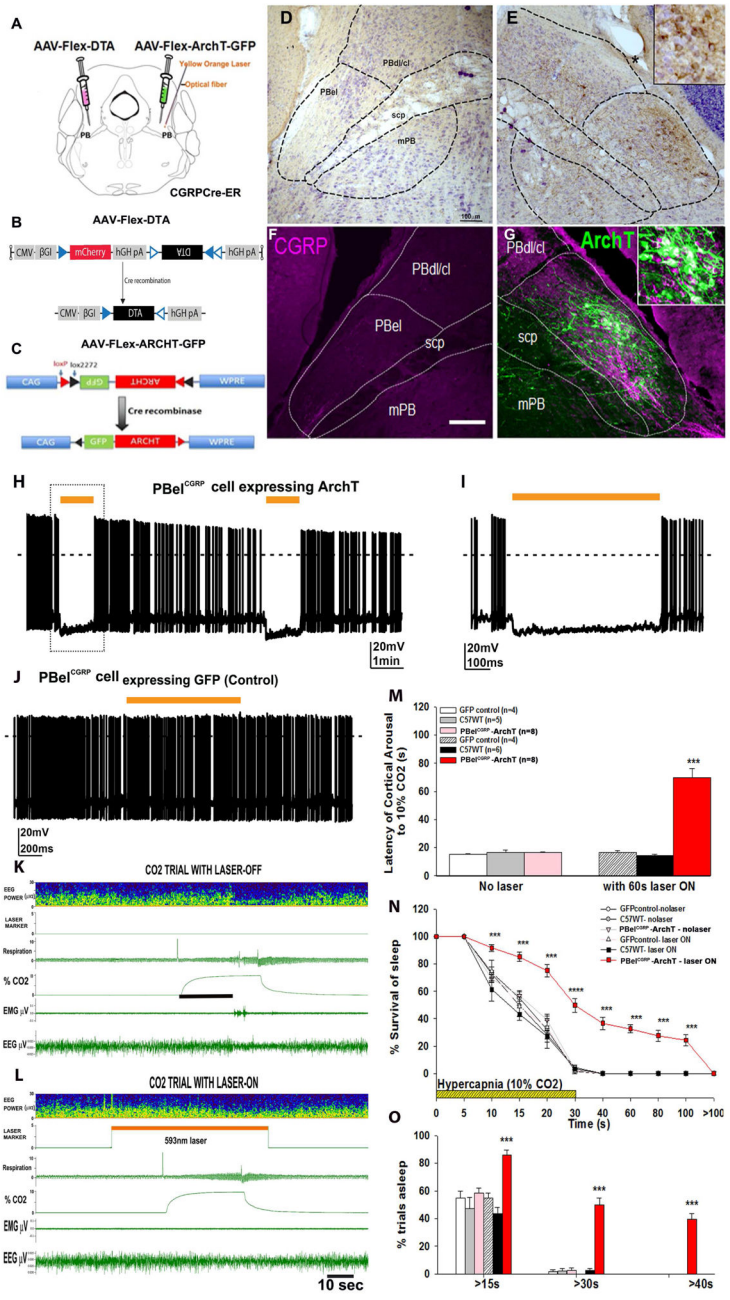

Figure 2. Optogenetic silencing of the PBel^{CGRP} neurons blocks hypercapnia induced arousal.< br>A, schematic design of optogenetic inhibition of PBel^{CGRP} neurons (green right), and genetically directed killing of these neurons on the left (pink). B shows diagrams of the AAV-Flex-DTA vector used for genetically directed cell killing and C illustrates the AAV-Flex-ArchT-GFP vector used for laser inhibition. CGRP neurons in the right PBel expressed ArchT, and an optical glass fiber inserted on the same side inhibited these neurons with 593 nm laser light. D,E Photomicrographs of coronal sections of a mouse brain immunostained for Green Fluorescent Protein (GFP; co-expressed with ArchT) and counter stained for Nissl. A magnified view of the ArchT expressing neurons is shown in the inset in E. An

asterisk shown in E marks the track of optical glass fiber. Absence of Nissl stained cells on the left side in the PBel in D and CGRP neurons on the left in F is due to ablation of $PBel^{CGRP}$ neurons by DTA. F and G are double-stained for CGRP (magenta) and GFP-ArchT (green), and on the right side (G) all the GFP-ArchT labeled neurons are CGRP positive (double-labeling is white).

Orange-light pulses inhibit firing of $PBel^{CGRP}$ neurons expressing ArchT in *in vitro*. (**H–I**) Whole-cell recordings from $PBel^{CGRP}$ neurons that express ArchT-GFP in current clamp mode. Orange-light pulses (60 s duration) hyperpolarize and silence action potential firing of CGRP neurons expressing ArchT (*panel H*: two 60 s light pulses separated by five minutes and *panel I*: expanded trace of the outlined region from panel H, shows the response to the first light pulse). J shows Orange-light pulses produce no changes in the firing rate of $PBel^{CGRP}$ neurons expressing GFP (mice injected with AAV-Flex-GFP).

Orange-light pulses prevent CO2 arousal (K, L) Representative recordings of EEG, EMG and respiration during the 10% CO2 stimulus in a CGRP-CreER mouse injected in PB with AAV-Flex-DTA on the left side and AAV-ArchT on the right side, without 593nm laser in K and with laser exposure for one minute beginning 20 sec before the CO2 stimulus in L. With no laser (K) the mouse awoke (denoted by sudden change in EEG power spectrum and EMG) at the latency of 18s (black bar) to CO2, but with laser inhibition of PBel, the mouse in this representative trial (L) did not wake up. M, Graphs comparing the latency of arousal (mean ± SEM) with and without laser to 30s of 10% CO2. Latency with the laser on was similar to animals that received no CO2 at all (cf. Fig. 4). N shows the survival of a NREM sleep bout during and after a hypercapnic stimulus with and without the laser. O shows the percentage of animals with arousals at 15, 30 and 40s in each group. (*** - $p < 0.001$, 1-way or repeated measures ANOVA followed by Holms-Sidak for multiple comparison). Scale in F = 100 μm. **Abbreviations**: PB, parabrachial nucleus, el, external lateral, cl, central lateral, and dl, dorsal lateral PB subnuclei; scp, superior cerebellar peduncle.

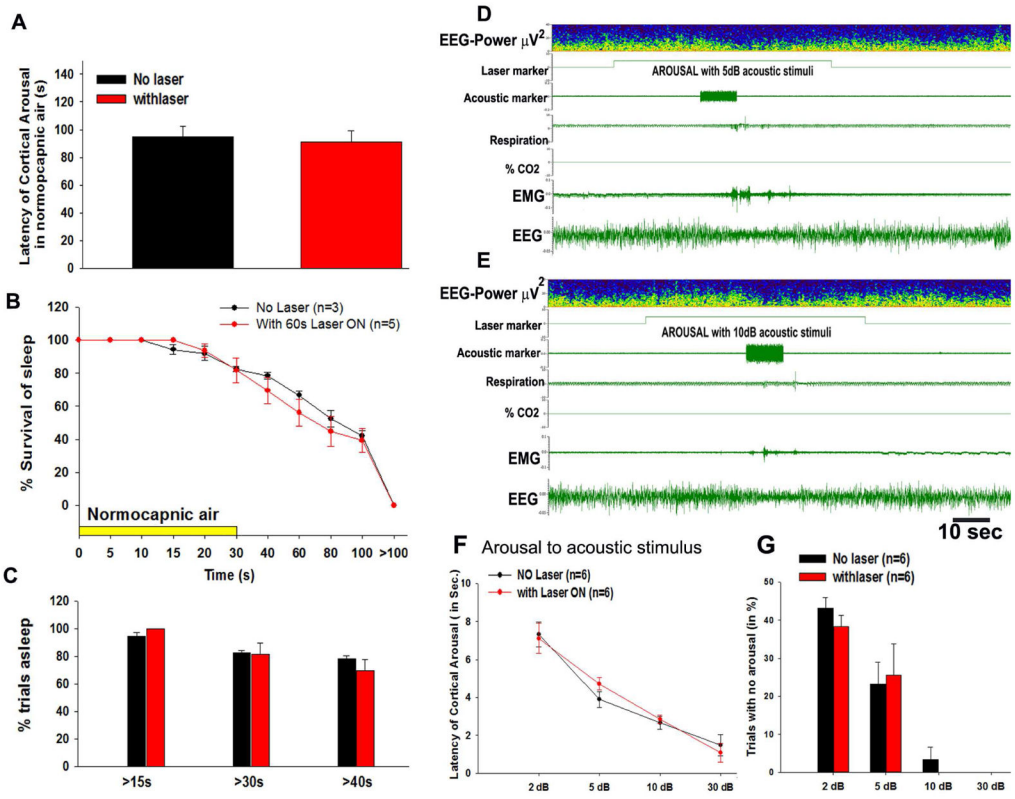

Figure 3. EEG arousals in response to normocapnic air and acoustic stimulus

A–C, Graphs as in Fig. 2 showing the latency to arousal (mean ± SEM) during the Laser-ON and Laser-OFF conditions in the presence of the normocapnic gas instead of CO2. The survival curves during the normocapnia air (B) and the arousal at the 15, 30 and 45s were comparable during laser ON and Laser OFF with normocapnic air. D,E, Representative figures showing normal arousals to the 5dB and 10dB 4 kHz acoustic stimulus even with Laser-ON. F, Latencies of cortical arousal (in sec; mean ± SEM) are compared at different sound intensities (x-axis) in the CGRP-CreER mice, which showed no significant difference in the latency to wake up to the sound, without laser (black) and with 60s Laser-ON (red), in animals in which CO2 arousal was suppressed in the Laser-ON condition. G, shows the percentage of trials which show arousal in response to different sound intensities (x-axis) in the CGRP-CreER mice in both laser-ON and laser-OFF conditions.

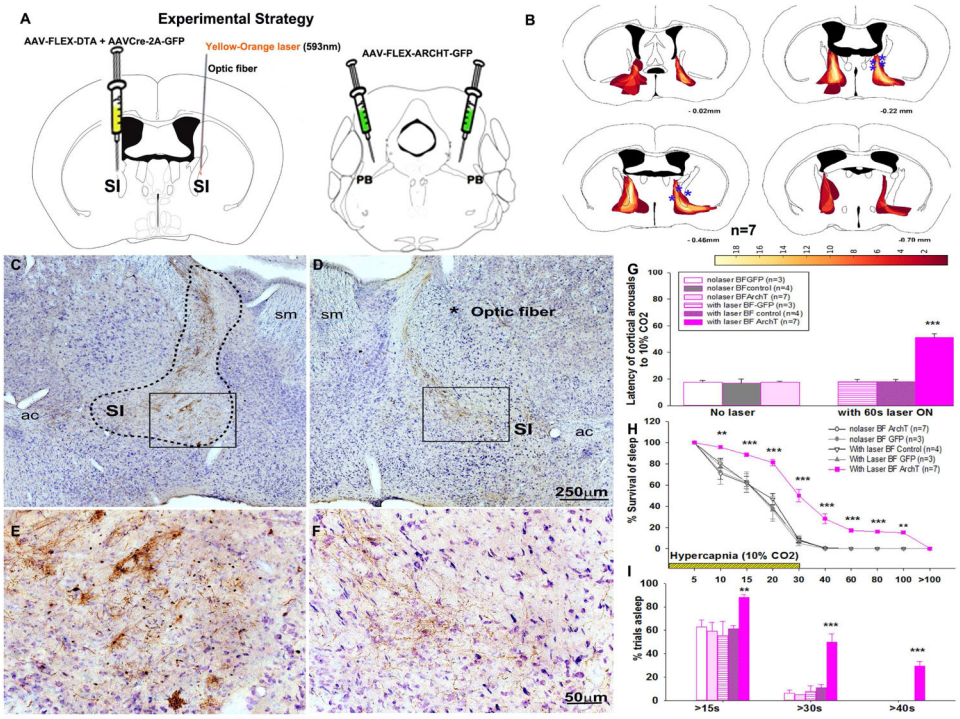

Figure 4. Optogenetic silencing of PBel^{CGRP} terminal fields in the BF block hypercapnia-induced arousal<

br>A is a schematic drawing of the optogenetic experiment. PB is injected bilaterally with AAV-Flex-ArchT-GFP to transfect PBel^{CGRP} neurons. BF neurons in the PBel^{CGRP} terminal field are deleted on the left and an optical fiber is implanted above them on the right to illuminate the terminals with 593 nm laser light. B shows a heat map of the lesions on the left and anterograde labeling of the terminal field on the right (optical fiber tips marked with blue asterisks) in 7 mice with correct targeting all of which showed responses to laser photoinhibition. C, D Photomicrographs showing the ArchT (immunostained for GFP) labeled fibers and terminals in the BF on each side of brain. On the left side (C,E) there is loss of large blue neurons in the terminal field, while on the right side the track of the optical fiber is seen as it penetrates the brain above the BF (D, tip of the fiber marked by asterisk). E, F are the magnified views of the lesioned (C) and the intact side (D) with ArchT terminals apposed to the intact cells in F. G–H, Graphs as in fig. 2 comparing the latency of arousal (mean ± SEM) with and without laser photoinhibition of the PBel^{CGRP} terminals in BF to 30s of 10% CO2; survival of NREM sleep bouts during and after a hypercapnic stimulus shown with and without the laser; and comparisons of the percent animals with failure to arouse at 15, 30 and 40s.

Abbreviations: ac, anterior commissure; SI, substantia innominata; sm, stria medullaris.

(***- P< 0.001, **- P<0.01, 1-way or repeated measures ANOVA followed by Holm-Sidak for multiple comparison).

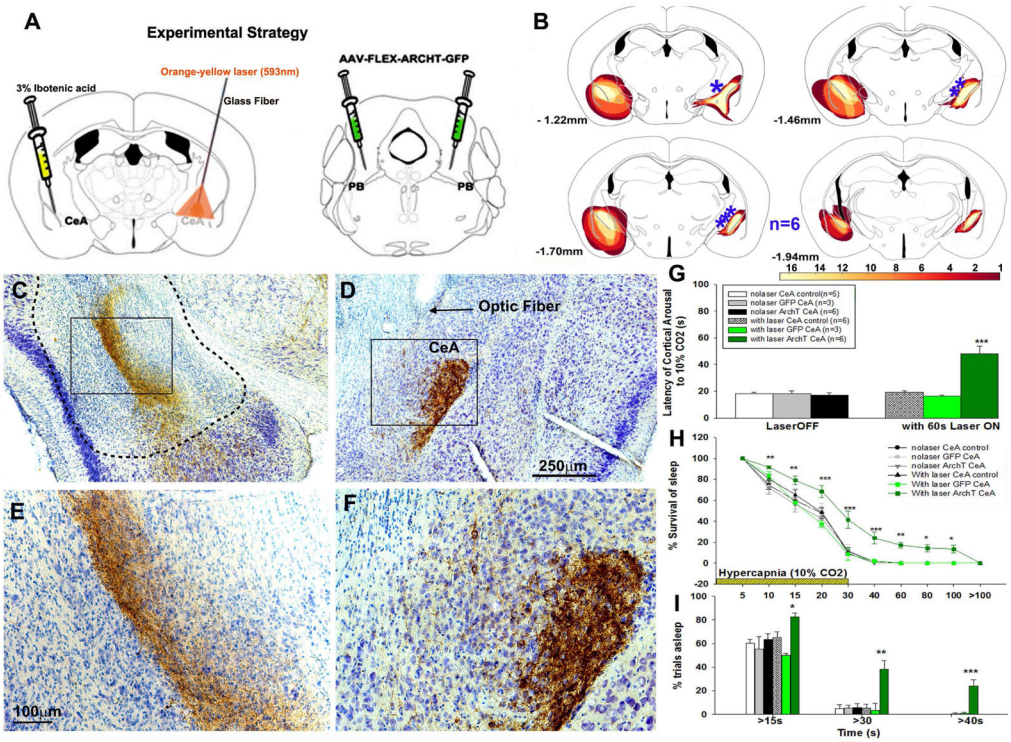

Figure 5. Optogenetic silencing of PBel^{CGRP} terminal fields in the CeA attenuate hypercapnia-induced arousal

A, schematic of the experimental design. PBel was injected bilaterally with AAV-Flex-ArchT-GFP, and the CeA was lesioned on the left side, and an optical fiber implanted above the CeA on the right side to expose the region to 593 nm laser light to inhibit the CGRP-PBel terminal field. Figure B, shows heat maps of both the lesions on the left and the anterogradely labeled terminal fields (with optic fiber tips marked by blue asterisks) on the right plotted for 6 mice with correct targeting, all of which showed suppression of CO2 arousal. C–F, photomicrographs showing the ArchT (brown immunostaining for GFP) labeled fibers and terminals in CeA on both sides. On the left side the PBel terminal field in the CeA is filled with small blue glial cells but depleted of large blue neuronal cell bodies (Nissl staining; marked by dashed line in C, higher magnification in E); on the intact right side the optical fiber track is seen (D, marked by arrow), and anterogradely labeled PBel^{CGRP} terminals can be seen densely innervating the large blue neurons of the CeA (higher magnification in F). G, Graph comparing the latency of arousal (mean ± SEM) with and without laser photoinhibition of the CeA terminals to 30s of 10% CO2. H, Survival of NREM sleep bouts during and after a hypercapnic stimulus shown with and without the laser. I shows the percent of animals with failure to arouse at 15, 30 and 40s.
(***- P< 0.001, **- P<0.01 and *- P<0.05, 1-way or repeated measures ANOVA followed by Holm-Sidak).

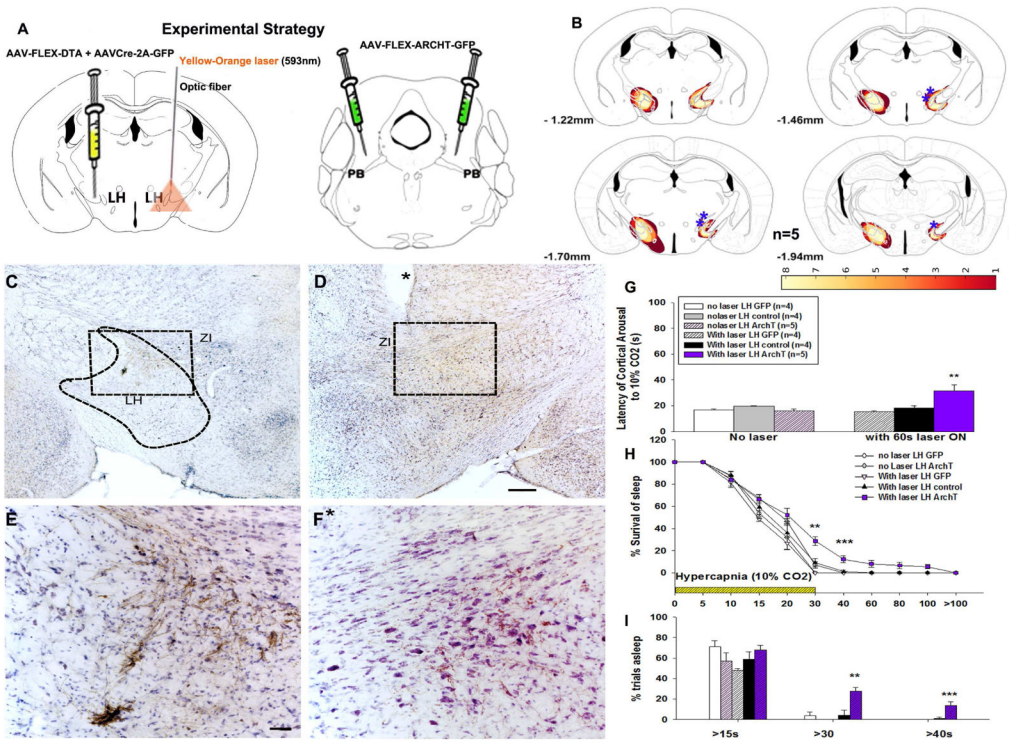

Figure 6. Optogenetic silencing of PBel^{CGRP} terminal fields in the LH attenuate hypercapnia-induced arousal

A, experimental design with injection of the PB with AAV-Flex-ArchT-GFP bilaterally, and then lesion of the PBel^{CGRP} terminal field in the left LH, and implanting an optical fiber on the right side targeting the contralateral LH with 593 nm laser light. B, heat maps showing lesions on the left side and CGRP terminal fields on the right (optical fiber tips marked by blue asterisks) for 5 mice with correct targeting, all of whom showed photoinhibition of CO2 arousal. C,D, Photomicrographs showing the ArchT (immunostained brown for GFP) labeled fibers and terminals in the LH on each side of the brain. The left LH shows the lesioned area with loss of large neurons on Nissl staining (marked by dashed line in C) involving the CGRP terminal area; the right side is intact with an optical fiber track targeting the LH (asterisk). E is a magnified view from C showing absence of large neurons due to lesion in the LHA; fusiform horizontally oriented neurons in the zona incerta (ZI) at the top of the frame are intact. F is magnified view of the intact side targeted by the glass-fiber, again showing the zona incerta at the top of the frame, and much larger multipolar LHA neurons in the lower half of the frame. G, Graph comparing the latency of arousal (mean ± SEM) with and without laser to 30s of 10% CO2. H, survival of sleep during and after a hypercapnic stimulus shown with and without the laser. J, Comparisons of percent of animals with failure to arouse at 15, 30 and 40s.

(** - $p < 0.001$; * - $p < 0.05$, 1-way or repeated measures ANOVA followed by Holm-Sidak for multiple comparison). Scale: C and D- 100 μm; E and F- 50 μm.

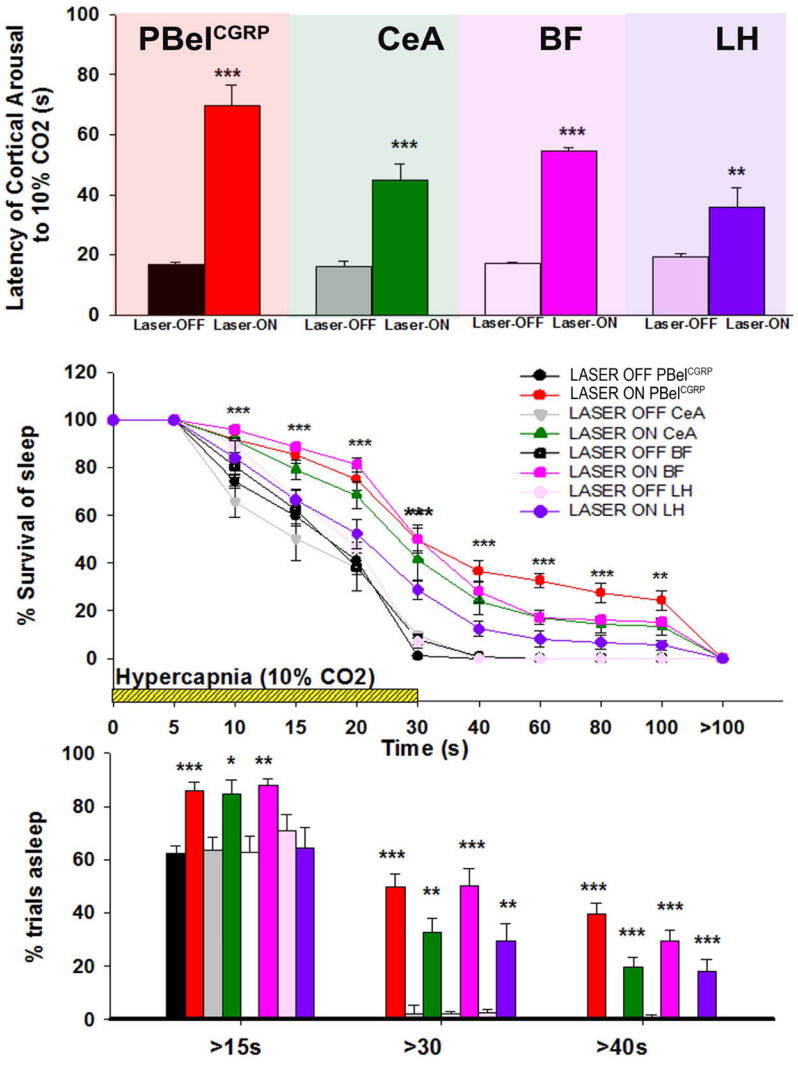

Figure 7. Comparing the effects of PBel^{CGRP} soma inhibition to that of PBel^{CGRP} terminals field inhibition

A, latency of arousal (mean ± SEM) during laser (593nm) induced inhibition of the PBel^{CGRP} neurons is compared with inhibition of the terminal fields in the BF, CeA and LH. B, survival of sleep curves during and after a hypercapnic stimulus shown with and without laser. C, comparisons of percent of animals with failure to arouse at 15, 30 and 40s. (*** - $p < 0.0001$; ** - $p < 0.001$; * - $p < 0.05$, 1-way or repeated measures ANOVA followed by Holm-Sidak for multiple comparison).

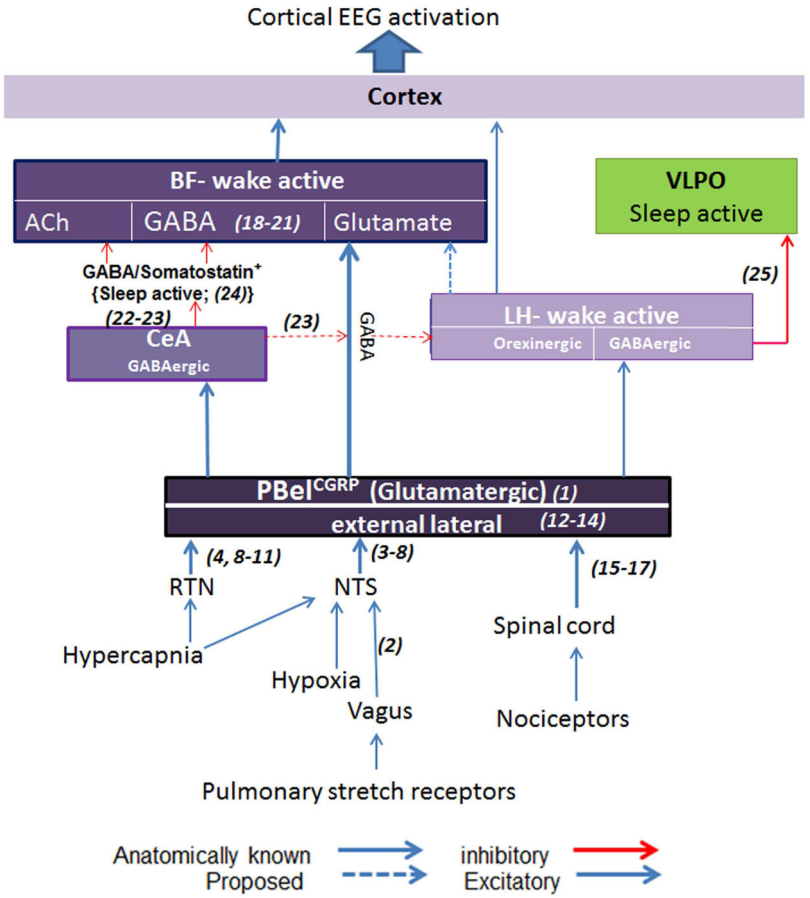

Figure 8. Putative neural circuitry regulating cortical arousals to hypercapnia

A schematic map of the proposed role of the PBel^{CGRP} neurons in regulating arousal with increasing levels of CO2 during apneas. PBel^{CGRP} neurons receive CO2, O2 and airway mechanoreceptor inputs, as well as inputs from other systems (e.g., nociceptors) that may degrade sleep. The PBel^{CGRP} neurons in turn project extensively to the lateral hypothalamus (LH), basal forebrain (BF), and central nucleus of amygdala (CeA). Our findings suggest that PBel^{CGRP} neurons mainly cause cortical arousal by projections to the BF, which has potent waking effects. Neurons in CeA do not have ascending projections to the cortex, but may cause arousal by means of projections to the BF and LH. Neurons in the LH have less effect on arousal, which may be mediated by projections to the cerebral cortex or the BF, but may also be due to inhibitory neurons contacting sleep-promoting neurons in the ventrolateral preoptic nucleus (VLPO).

Abbreviations: Retrotrapezoid nucleus (RTN); nucleus of solitary tract (NTS).

References in the figure (all supplied in the reference list): (1) (Yasui et al., 1991); (2) (Kalia and Richter, 1988); (3) (Berquin et al., 2000); (4) (Haxhiu et al., 1996); (5) (Moreira et al., 2006) (6) (Panneton and Loewy, 1980); (7) (Song et al., 2010)); (8) (Yokota et al., 2015); (9) (Bochorishvili et al., 2012); (10) (Guyenet et al., 2010) (11) (Mizusawa et al., 1995); (12) (Bernard et al., 1993); (13) (Saper and Loewy, 1980); (14) (Saper, 1982); (15) (Carter et al., 2013); (16) (Carter et al., 2015) (17) (deLacalle S. and Saper, 2000); (18) (Anaclet et al., 2015); (19) (Fuller et al., 2011); (20) (Kaur et al., 2008); (21) (Kim et al.,

2015); (22) (Gastard et al., 2002); (23) (Jolkkonen et al., 2001); (24) (Xu et al., 2015); (25) (Venner et al., 2016).